Infrared and Raman Spectroscopy of Biological Materials

edited by

Hans-Ulrich Gremlich

Novartis Pharma AG
Basel, Switzerland

Bing Yan

ChemRx Advanced Technologies, Inc.
South San Francisco, California

MARCEL DEKKER, INC. NEW YORK • BASEL

Copyright © 2000 by Marcel Dekker, Inc. All Rights Reserved.

Marcel Dekker, Inc.

Toll-Free Phone: 1-800-228-1160

Send your order and payment to:

Marcel Dekker, Inc.
Journal Customer Service
P.O. Box 5017
Monticello, NY 12701-5176
Phone: (845) 796-1919
Fax: (845) 796-1772

Or by e-mail to:

jrnlorders@dekker.com

For claims and inquiries:

custserv@dekker.com

Send your request for a complimentary sample copy or advertising information to:

Marcel Dekker, Inc.
Promotion Department
270 Madison Avenue
New York, NY 10016-0602
Phone: (212) 696-9000
Fax: (212) 685-4540

Or by e-mail to:

journals@dekker.com

To purchase offprints of articles that appear in any Marcel Dekker, Inc. journal:

offprints@dekker.com

To inquire about special sales and bulk purchases of Marcel Dekker, Inc. journals:

bulksale@dekker.com

A COMPLETE LISTING OF **ABSTRACTS** FOR CURRENT ISSUES,
TABLES OF CONTENTS, AND **INSTRUCTIONS TO AUTHORS**
REGARDING MANUSCRIPT PREPARATION AND SUBMISSION FOR ALL MARCEL DEKKER, INC.
JOURNALS CAN BE FOUND ON OUR WEBSITE AT:

http://www.dekker.com

5

Biophysical Infrared Modulation Spectroscopy

Urs P. Fringeli and Dieter Baurecht
University of Vienna, Vienna, Austria

Hans H. Günthard
Swiss Federal Institute of Technology, Zurich, Switzerland

1 INTRODUCTION

Modulation spectroscopy or modulated excitation (ME) spectroscopy can always be applied if a system admits a periodic alteration of its state by the variation of an external parameter, such as temperature (T), pressure (p), concentration (c), electric field (E), electric potential (Ψ), radiant power (Φ), or mechanical force (F). The response of the system to ME will also be periodic, exhibiting the same frequency as the stimulation. In case of a nonlinear system, the response to a sinusoidal stimulation will also contain multiples of the fundamental frequency. After an initial period of stimulation, the system will reach the stationary state, which is characterized by periodic alterations around a constant mean. In case of incomplete reversibility, e.g., the existence of an irreversible exit in the reaction scheme, the signal amplitudes of the initial components and of the intermediate species will decline as the system is approaching its final state.

Phase-sensitive detection (PSD) is used for the evaluation of amplitudes and phase lags of the periodic system response. In a simple view, PSD applied to data from a spectroscopic ME experiment results in a special kind of difference spectra between excited and nonexcited states. Let us consider a system that is stimulated by a sinusoidally oscillating external parameter. During one half-wave, one has excitation followed by relaxation in the other. In the stationary state, this alteration between excitation and relaxation may be repeated as many times as necessary in order to obtain a good signal-to-noise (S/N) ratio of the modulation

spectra. Moreover, it should be noted that PSD is a narrowband detection; i.e., noise contributes only from a frequency range that is close to the stimulation frequency ω.

Since the periodic system response is evaluated automatically within each period of stimulation, instabilities of the spectrometer, the environment, and the sample are much better compensated than with conventional techniques, where a reference spectrum has to be stored at the beginning of the experiment. As a consequence, the ME technique generally leads to high-quality background compensation with a low noise level, resulting in enhanced sensitivity by at least one order of magnitude.

So far, ME spectroscopy appears as a special type of difference spectroscopy. This is true if the frequency of stimulation is slow compared to the kinetics of the response of the stimulated system. However, if one or more relaxation times of the externally excited process fulfill the condition $0.1 < \omega \cdot \tau_i < 10$, where ω denotes the angular frequency of stimulation and τ_i is the ith relaxation time of the system, significant phase lags φ_i between stimulation and sample responses will occur. As will be derived in Section 6, phase lag and relaxation time are related by $\varphi_i = \arctan(-\omega \cdot \tau_i)$. This phenomenon is paralleled by damping of the response amplitudes A_i. Both signify the underlying reaction scheme and the associated rate constants of the stimulated process (1). In this case, selectivity of ME spectroscopy, e.g., with respect to single components in heavily overlapping absorption bands, is significantly higher than that achievable by normal difference spectroscopy. The reason is the typical dependence of phase lags φ_i and amplitudes A_i on the modulation frequency ω. If a set of absorption bands of a modulation spectrum exhibits the same phase lag φ_i, it is considered a correlated population. Such a population consists, e.g., of molecules or parts of them that are involved in the same reaction step. The assignment of a group of absorption bands in a modulation spectrum to a population is considered to be validated if upon changing the stimulation frequency ω all these bands exhibit further on the same dependence with respect to phase lag $\varphi_i(\omega)$ and amplitude $A_i(\omega)$.

Moreover, the dependence of phase lag and amplitude on ω may be calculated based on a given reaction scheme. Analytical expressions for a simple reversible reaction $A_1 \rightleftarrows A_2$ are given in Section 6. Obviously, ME spectroscopy enables a very rigorous test of the significance of a reaction scheme, since consistency of experimental data with theory derived from a given reaction scheme must hold over the whole frequency range of stimulation. Theoretically, as will be shown in Sec. 6, modulation spectroscopy and relaxation spectroscopy (2,3) have the same information content regarding kinetic parameters. The access to these parameters, however, is quite different. One relaxation experiment may result in the whole information, because broad band stimulation and detection is applied. As a consequence, a correspondingly high noise level must be expected. On the other hand, ME spectroscopy, as narrow band technique, requires a series

of experiments at different excitation frequencies. As a consequence, the signal-to-noise (S/N) ratio is significantly enhanced, and moreover, phase sensitive detection (PSD) of the system response, which is equivalent to Fourier analysis, enables unambiguous experimental detection of non-linearities of the stimulated system. These may result e.g. from 2nd order reactions, phase transitions and/or cooperative phenomena. Therefore, ME spectroscopy enables a more rigorous validation of experimental data, since the system response at any frequency must be consistent with the reaction scheme underlying the kinetic analysis. The price to pay for this advantage, however, are a more complicated theoretical approach for the evaluation of kinetic parameters and more time consuming experiments.

In this chapter we will report on temperature-modulated excitation (T-ME) of poly-L-lysine, on concentration-modulated excitation (c-ME) of acetylcholinesterase (AChE) and arachidic acid (ArAc), on electric field–modulated excitation (E-ME) of poly-L-lysine, and of UV-VIS–modulated excitation (Φ-ME) of pyrocatechol.

Two-dimensional IR spectroscopy (4) as a tool of ME data presentation is discussed in Sec. 4; Sec. 5 deals with signal processing of data obtained by ME. Finally, as an example, the modulation spectroscopic approach to kinetic data of the simple reversible reaction $A_1 \rightleftarrows A_2$ is demonstrated.

2 METHODS OF MODULATED EXCITATION

Modulation of external parameters such as temperature (T), pressure (p), electric potential (Ψ), electric field (E), concentration (c) of a substrate, and excitation of electronic states in molecules by modulated UV-VIS radiation (Φ) may lead to periodic concentration changes of the reactants in chemical, biochemical, or biological systems. Mechanical strain modulation applied to a polymer sample may be used to study strain-induced structural changes in the sample. The mean concentrations corresponding to the stationary state are given by the equilibrium concentrations corresponding to the mean values of the external parameters. Using the general symbol η to denote the external parameter used for ME, one obtains in case of a harmonic stimulation

$$\eta(t) = \eta_0 + \Delta\eta_0 + \Delta\eta_1 \cos(\omega t + \theta) \tag{1}$$

$\Delta\eta_0$ denotes the offset of the stationary state with respect to the initial state; i.e., $\eta_0 + \Delta\eta_0$ is the average value of the parameter in the stationary state. $\Delta\eta_1$ is the modulation amplitude of the corresponding parameter. θ denotes the phase of the stimulation, a parameter that is under experimental control by the operator. The shape for harmonic stimulation with $\theta = \pi$ is shown in Fig. 1. The principle components of an ME spectrometer are depicted in Fig. 2.

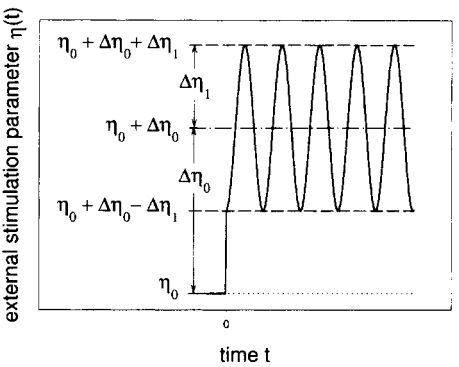

Fig. 1 External harmonic modulated excitation according to Eq. (1). η denotes any external parameter. η_0 is the initial value at the beginning of the experiment. $\Delta\eta_0$ is the offset from initial state to stationary state, which corresponds to the equilibrium state at the parameter setting $\eta_0 + \Delta\eta_0$. $\Delta\eta_1$ denotes the modulation amplitude. θ is the phase angle, determining the onset of the stimulation. With $\theta = \pi$, stimulation starts at the minimum value of the parameter.

2.1 Temperature-Modulated Excitation (T-ME)

For an analytical description of the influence of the external parameter T on rate constants, one may use the approximation by Arrhenius, Eq. (2):

$$k = Ae^{-E_a/RT} \tag{2}$$

By introducing Eq. (1) into Eq. (2), one obtains

$$k(t) = Ae^{-E_a/(R(T_0+\Delta T_0+\Delta T_1\cos(\omega t+\theta)))} \tag{3}$$

For small perturbations, i.e., ΔT_0, $\Delta T_1 \ll T_0$, Eq. (3) may be approximated by the linear part of a Taylor series expansion at T_0:

$$k(T(t)) = k(T_0) + k(T_0)\frac{T_A}{T_0^2}(\Delta T_0 + \Delta T_1 \cos(\omega t + \theta)) \tag{4}$$

$T_A = E_a/R$ will be referred to as *Arrhenius temperature*. Under these conditions, Eq. (4) may be used to get the relevant rate equations. An example will be given in Sec. 6.

It should be noted that if the system undergoes a phase transition or is involved in a cooperative process, this approach will still hold. However, more complicated reaction schemes have to be used. Cooperative phenomena have been described, e.g., by Hill (6) and Monod et al. (7).

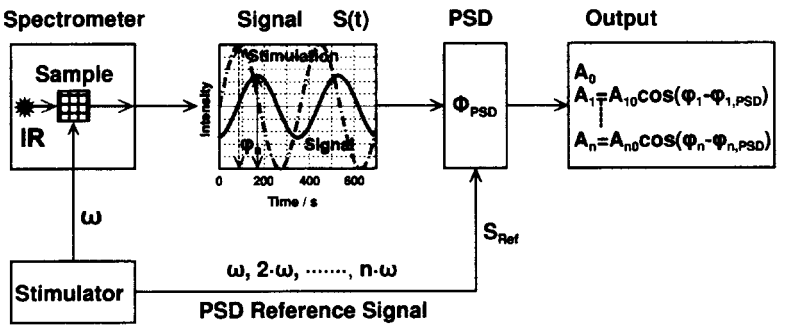

Fig. 2 Schematic setup for modulated excitation (ME) spectroscopy. A periodic excitation is exerted on the sample with frequency ω. The sample response $S(t)$, as sensed by IR radiation, contains the frequency ω and higher harmonics at wavelengths that are significant for those parts of the sample that have been affected by the stimulation. Selective detection of the periodic sample responses is performed by phase-sensitive detection (PSD), resulting in the DC output A_n of fundamentals ω ($n = 1$) and their harmonics $n\omega$ ($n = 2, 3, \ldots$), as well as the phase shifts φ_n between the nth harmonic and the stimulation. This phase shift is indicative of the kinetics of the stimulated process and of the underlying chemical reaction scheme. Since the PSD output A_n ($n = 1, 2, \ldots, n$; frequency $n \cdot \omega$) is proportional to $\cos(\varphi_n - \phi_{n,PSD})$, absorption bands featuring the same phase shift φ_n are considered to be correlated, i.e., to be representative of a population consisting of distinct molecules or molecular parts. $\phi_{n,PSD}$ is the operator-controlled PSD phase setting. Because of the cosine dependence, different populations will have their absorbance maxima at different $\phi_{n,PSD}$ settings, thus enabling selective detection. Moreover, in the case where $0.1 < \omega \cdot \tau_i < 10$ (τ_i denotes the ith relaxation time of the system), φ_n becomes ω dependent, $\varphi_n = \varphi_n(\omega)$. The spectral information can then be spread in the $\phi_{n,PSD}$-ω-plane, resulting in a significant enhancement of resolution with respect to standard difference spectroscopy and conventional time-resolved spectroscopy. (Reproduced from Ref. 5 by permission of Academic Press.)

2.2 Pressure-Modulated Excitation (p-ME)

In the Arrhenius model, Eq. (2), the rate constant is considered to be pressure independent. Therefore, a refined calculation of the rate constant is required. Using the activated complex theory (transition-state theory) (8), one obtains for the rate constant k_+

$$k_+ = \kappa \frac{kT}{h} K^{\neq} = \kappa \frac{kT}{h} e^{-\Delta G^{\neq}/RT} \tag{5}$$

κ is called the *transmission coefficient*. Its value is generally between 0.5 and 1. k and h mean the Boltzmann and Planck constants, respectively. $K^{\neq}$ is the equilibrium constant of the reaction from the initial to the transition state, and

$\Delta G^{\neq}$ denotes the corresponding free enthalpy of reaction (Gibbs energy). The dependence of k_+ on pressure p results from the dependence of $\Delta G^{\neq}$ on p; i.e., $\partial \Delta G^{\neq}/\partial p = \Delta V^{\neq}$. Since small pressure-induced changes of $\Delta G^{\neq}$ are expected, a linear dependence may be assumed, resulting from Eq. (5):

$$k_+(p) = \kappa \frac{kT}{h} e^{-(\Delta G^{\neq}(p_0) + \Delta V^{\neq}(p(t)-p_0))/RT} = k_+(p_0) e^{\Delta V^{\neq}(p(t)-p_0)/RT} \tag{6}$$

Furthermore, since $\Delta V^{\neq}(p(t) - p_0)/RT \ll 1$, a linear influence of pressure on rate constant may be assumed. Therefore, Eq. (6) results after insertion of the oscillating external pressure according to Eq. (1):

$$k_+(\mathrm{p}) = k_+(p_0)\left(1 + \frac{\Delta V^{\neq}}{RT}(p(t) - p_0)\right) = k_+(p_0) + k_+(p_0)\frac{\Delta V^{\neq}}{RT}(\Delta p_0 + \Delta p_1 \cos(\omega t + \theta)) \tag{7}$$

2.3 Electric Field–Modulated Excitation (E-ME)

Chemical reactions may be influenced by strong electric fields ($E \approx 10^4$ V/m and larger) via dipole-field interaction. If $\vec{M}_i$ denotes the dipole moment per mole of a species A_i that is exposed to the electric field $\vec{E}$, the chemical potential μ_i will be altered by the energy $-(\vec{M}_i \cdot \vec{E})$ (Stark effect). The corresponding change per extent of reaction is then given by $-(\Delta\vec{M} \cdot \vec{E})$, where $\Delta\vec{M} = \sum \nu_i \vec{M}_i$ denotes the reaction dipole moment, which is assumed to be composed of a static part $\Delta\vec{M}_{\mathrm{stat}}$ and an induced part $\Delta\vec{M}_{\mathrm{ind}}$. The latter is given by $\Delta\vec{M}_{\mathrm{ind}} = \sum \nu_i \alpha_i \vec{E} = \Delta\alpha\vec{E}$. α_i is the electric polarizability tensor of A_i, and ν_i is the corresponding stoichiometric number, which is defined as a negative or positive number, depending on whether A_i is a reactant or a product, respectively. Thus $\Delta\alpha$ denotes the electric reaction polarizability. Making use of Eq. (5), one obtains for the rate constant

$$k_+(\vec{E}) = \kappa \frac{kT}{h} e^{-(\Delta G^{\neq}(\vec{E}=0) - (\Delta\vec{M}^{\neq}_{\mathrm{stat}} + \Delta\vec{M}^{\neq}_{\mathrm{ind}})\cdot\vec{E})/RT} = k_+(\vec{E} = 0) \cdot e^{\Delta\vec{M}^{\neq}_{\mathrm{stat}}\vec{E}/RT} \cdot e^{\Delta\alpha^{\neq}\vec{E}^2/RT} \tag{8}$$

The two exponentials on the right-hand side of Eq. (8) describe the influence of the electric field on the rate constant via the interaction with static and induced dipole moments of the reactants, respectively. For the sake of simplicity we assume induced dipole moments to have the same direction as the electric field.

In this case, which holds exactly for spherical symmetry, α_i and $\Delta\alpha$ become scalars. The two exponentials may now be expanded into Taylor series until the first electric field–dependent term:

$$e^{\Delta\vec{M}^{\neq}_{stat}\vec{E}/RT} \approx 1 + \frac{\Delta M^{\neq}_{stat}\cos(\Delta\vec{M}^{\neq}_{stat}\vec{E})}{RT}E \quad \text{and} \quad e^{\Delta\alpha^{\neq}\vec{E}^2/RT} \approx 1 + \frac{\Delta\alpha^{\neq}}{RT}E^2 \tag{9}$$

Insertion of Eq. (9) into Eq. (8) results in

$$k_+(\vec{E}) \approx k_+(0)\cdot\left(1 + \frac{\Delta M^{\neq}_{stat}\cos(\Delta\vec{M}^{\neq}_{stat}\vec{E})}{RT}E + \frac{\Delta\alpha^{\neq}}{RT}E^2 + \frac{\Delta\alpha^{\neq}\Delta M^{\neq}_{stat}\cos(\Delta\vec{M}^{\neq}_{stat}\vec{E})}{(RT)^2}E^3\right) \tag{10}$$

Let's consider now an oscillating electric field according to Eq. (1):

$$E(t) = E_0 + \Delta E_0 + \Delta E_1\cos(\omega t + \theta) \tag{11}$$

Insertion of Eq. (11) into Eq. (10) results in the time dependence of the alteration of the rate constant due to an oscillating external electric field. It should be noted that according to Eqs. (8) and (9), the interaction of the electric field of frequency ω with an induced reaction dipole will result in a response of 2ω as the lowest-frequency component. No fundamental frequency ω should result. However, a response with frequency ω may be assumed to result from electric field interaction with a static reaction dipole. Since PSD can discriminate between these two signals (see Sec. 5), it offers a powerful tool for reaction mechanistic analysis.

For the sake of completeness it should be mentioned that an exclusive 2ω response to a harmonic stimulation will also be observed when a static molecular dipole reorients synchronously and symmetrically with an electric field oscillating about zero. This is the case because parallel and antiparallel alignment of a molecule results in the same optical absorption.

2.4 Concentration-Modulated Excitation (c-ME)

Concentration-modulated excitation (c-ME) is performed by periodic alteration of the concentration of an effector molecule in the spectroscopic flow-through cuvette. In contrast to the three cases discussed earlier, c-ME acts directly on the system by disturbing the chemical equilibrium or stationary state. Again, the time course of the stimulating concentration may be described by Eq. (1):

$$c(t) = c_0 + \Delta c_0 + \Delta c_1\cos(\omega t + \theta) \tag{12}$$

$c_0 + \Delta c_0$ denotes the stationary concentration, and Δc_1 is the amplitude of the modulated concentration.

2.5 UV-VIS–Modulated Excitation (Φ-ME)

UV-VIS–modulated excitation (Φ-ME) is performed by exposition of the system to a modulated radiant power $\Phi(t)$ [W]. The contribution of Φ-ME to the overall rate of species A_i is then given by

$$\dot{c}_{i,\Phi} = -\Phi(t) w_i c_i \tag{13}$$

w_i denotes the transition probability [W^{-1} s^{-1}] and c_i is the molarity of A_i. According to Eq. (1), the radiant power may be expressed by

$$\Phi(t) = \Phi_0 + \Delta\Phi_0 + \Delta\Phi_1 \cos(\omega t + \theta) \tag{14}$$

For Φ-ME in general, $\Phi_0 = 0$ and $\Delta\Phi_0 = \Delta\Phi_1$, which means that flux modulation occurs around $\Phi_{mean} = \Delta\Phi_0$ between $\Phi_{min} = 0$ and $\Phi_{max} = 2\Delta\Phi_0$. $\Phi(t)w_i$ acts like a rate "constant" of a first-order reaction describing electronic excitation (pumping) of species A_i. According to a given reaction scheme, Φ-ME is expressed by the matrix **W** of transition probabilities induced by the UV-VIS field. This matrix has to be added to the well-known matrix **K** of thermal transition probabilities (matrix of rate constants), as demonstrated by Forster et al. (9) and discussed in Sec. 3.4.

2.6 Mechanical Strain–Modulated Excitation (S-ME)

Polymer films change molecular ordering upon stretching, as demonstrated by x-ray diffraction (10). Oscillatory mechanical strain was exerted on thin polymer films in order to detect structural changes in thin polymer films by transmission Fourier transform infrared (FT-IR) modulation spectroscopy (4,11). More recently, it was shown that p-ME of polymer samples on an attenuated total reflectance (ATR) crystal may result in similar structural information as S-ME, however, with more freedom concerning sample size and shape (12).

2.7 Polarization Modulation (PM)

Polarization modulation (PM) does not belong to the group of external excitation techniques; however, it also makes use of phase-sensitive detection (PSD) to enhance sensitivity. Phase modulation in combination with infrared reflection absorption spectroscopy (IRRAS) leads to enhanced instrumental stability and background compensation, which is advantageous when working with very thin samples on metal or even at the air–water interface. At about 50 kHz, PM is achieved by means of a photoelastic modulator (PEM). On a metal substrate, the sample will absorb light only in the ∥-polarized half-wave; the ⊥-polarized half-wave of the signal is therefore representative of the background. Subtraction is performed by lock-in technique (PSD) within each PM cycle, i.e., 50,000 times

per second. As a consequence, environmental and instrumental contributions are largely compensated (13,14).

3 EXAMPLES

3.1 Temperature-Modulated Excitation (T-ME) of Poly-L-lysine

Since the pioneering infrared work in the early 1950s (15,16), it has been known that typical amide group vibrations can be used to get information on protein and polypeptide secondary structure. In this context, poly-L-lysine (PLL) played an important role because of its ability to assume helical as well as antiparallel β-pleated sheet conformation, depending on the external conditions. Therefore PLL was used as a reference for protein amide group vibrational studies (17). Although helix and antiparallel β-pleated sheet as boundary states are confirmed by different experimental techniques, little is still known on the nature of the folding process. Application of T-ME has given evidence that intermediate species are accessible by this technique (18).

These experiments were performed with a poly-L-lysine film cast on an ATR plate (internal reflection element, IRE) and hydrated with D_2O (80% rel. humidity, 28°C). The sample was then exposed to a periodic temperature variation of ±2°C at a mean temperature of $\bar{T}$ = 28°C. According to Eq. (1), these conditions corresponded to T_0 = 26°C and $\Delta T_0 = \Delta T_1$ = 2°C. Slow modulation periods in the range of 2–15 min had to be applied in order to fulfill the optimum condition for modulation spectroscopy, namely, $\omega\tau \approx 1$, where ω denotes angular frequency and τ is relaxation time. A schematic drawing of the ATR cuvette used in the experiment is shown in Fig. 3.

The results obtained from T-ME with a 14.7-min period after phase-sensitive detection (PSD) are shown in Fig. 4. Part A shows the stationary spectrum and part B the phase-resolved spectra of the system response at the fundamental frequency ω. The numbers indicated on the spectra denote the phase settings ϕ^{PSD} at the phase-sensitive detector, which is a parameter under control of the operator. The ME spectra shown in Fig. 4B may be expressed by Eq. (15), which holds for the fundamental frequency ω. For more detailed information see Sec. 5.

$$\begin{aligned} A(\tilde{\nu}, \phi^{PSD}) &= A(\tilde{\nu}) \cdot \cos(\varphi_{\text{apparent}}(\tilde{\nu}) - \phi^{PSD}) \\ &= \sum_{i=1}^{N} A_i(\tilde{\nu}, \phi^{PSD}) = \sum_{i=1}^{N} A_i(\tilde{\nu}) \cdot \cos(\varphi_i - \phi^{PSD}) \end{aligned} \tag{15}$$

$A(\tilde{\nu}, \phi^{PSD})$ is referred to as *modulation spectrum*, which is the superposition of N component spectra $A_i(\tilde{\nu})$. Each component spectrum $A_i(\tilde{\nu})$ is characterized by the same phase angle φ_i of its absorption bands. Consequently, this set of bands

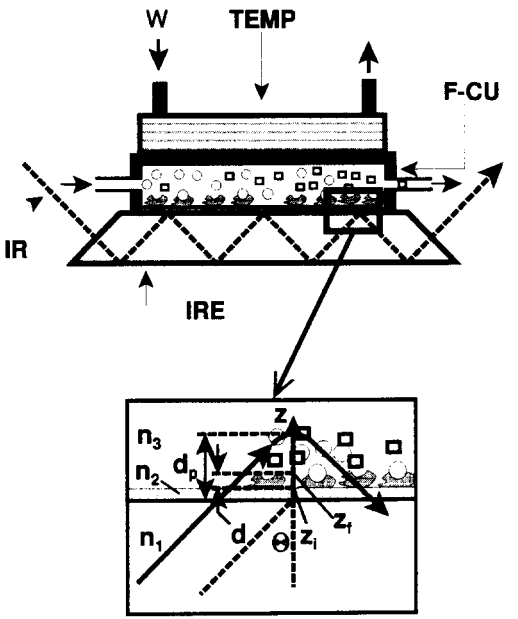

Fig. 3 IR ATR setup for T-ME experiments under controlled relative humidity. Flow-through cuvette (F-CU) thermostated (TEMP) by water circulation. Alternatively, two thermostats operated at $T_0 = 26°C$, and $T_0 + 2\Delta T_1 = 30°C$, respectively, are connected under computer control to the inlet (W) of the heat exchanger on the cuvette. The modulation period was between 2 to 15 min. The trapezoidal internal reflection element (IRE) was coated by a thin PLL layer spread from a solution in alcohol. D_2O humidified air (80% of r.h.) was circulated through the sealed cuvette.

may be considered to be correlated, i.e., to belong to a population of molecules or functional groups featuring the same kinetic response to the external stimulation. In such a population all absorbance bands exhibit the same dependence on the PSD phase setting ϕ^{PSD}. The amplitudes become maximum for $(\varphi_i - \phi^{PSD}) = 0°$, minimum (negative) for $(\varphi_i - \phi^{PSD}) = 180°$, and zero for $(\varphi_i - \phi^{PSD}) = 90°$ or 270°. Obviously, ϕ^{PSD} can be used to sense the overall phase angle $\varphi_{\text{apparent}}$, which depends on the wavenumber $\tilde{\nu}$. It enables only direct accesss to the phase angle φ_i of a population of absorption bands if there is no overlap with bands of a different population. The most accurate way to determine φ_i is achieved by line shape analysis of the whole set of phase-resolved spectra shown in Fig. 4B, followed by fitting a phase-resolved set of corresponding bands according to Eq. (15). For an example, the reader is referred to Ref. 18.

Although the spectral resolution of 4 cm^{-1} was the same for both stationary and modulation spectra, the first impression on comparing Fig. 4A with Fig.

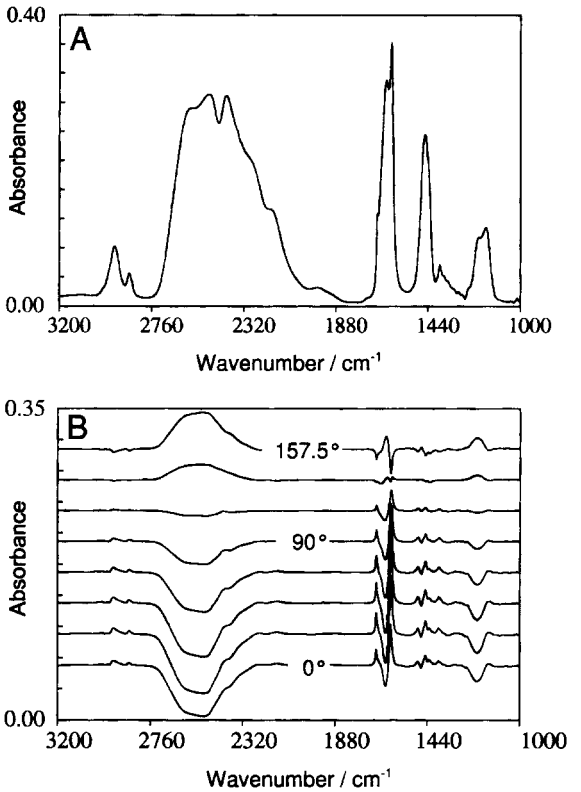

Fig. 4 Parallel polarized T-ME FT-IR spectra of a poly-L-lysine (PLL) deuterobromide film hydrated with D_2O (80% rel. hum., 28°C). The film was deposited on a CdTe ATR plate. A rectangular temperature stimulation was applied with a period of 14.7 min (ω = 0.427 min^{-1}) at $\bar{T}$ = 28°C ± 2°C. Angle of incidence: θ = 45°; mean number of internal reflections: N = 9–10. (A) Stationary part of the T-ME-IR spectrum of PLL. (B) Set of phase-resolved T-ME-IR spectra after phase-sensitive detection (PSD) at phase settings ϕ_{PSD} = 0°–157.5° (phase resolution 22.5°) with respect to the T-stimulation. ϕ_{PSD} = 0° means in phase, with temperature switching from 26°C to 30°C. Heat transfer from the thermostats to the sample resulted in an additional phase lag of ϕ_T = 25°. (Reproduced from Ref. 18 by permission of the American Chemical Society.)

4B is that modulation spectra are significantly better resolved. Since modulation spectra reflect only species that are involved in the stimulated process, band overlap may be drastically reduced, as in this case. Furthermore, Fig. 4B shows that not only the intensity but also the shape of phase-resolved spectra is changing with ϕ^{PSD}-setting. This is an unambiguous indication of the existence of populations of conformational states featuring different phase angles φ_i, which means

having different kinetic responses with respect to the stimulation. Extraction of these populations according to Eq. (15) enables the assignment of intermediate species in the amide I′ (1700–1600-cm^{-1}) and amide II′ (1500–1400-cm^{-1}) regions. For more details the reader is referred to Ref. 18.

As an example of a correlated population, the behavior of CH_2 stretching of the lysine side chain and the secondary structure of PLL should be mentioned. The weak absorption bands at 2865 cm^{-1} and 2935 cm^{-1} result from symmetric and antisymmetric stretching of these CH_2 groups. They are shifted by approximately 3 cm^{-1} toward lower wavenumbers if compared to the corresponding bands in the stationary state (Fig. 4A). This finding is indicative of a conformational change of a hydrocarbon chain from gauche defects into trans conformations (19,20); i.e., the chain is elongated. The phase of the CH_2 bands is found to be the same (correlated) as that of the antiparallel β-pleated sheet structure (amide I′ bands at 1614 cm^{-1} and 1685 cm^{-1}). We conclude, therefore, that the conversion of PLL from helix to β-sheet is paralleled by a conformational change of the lysine side chain from a bent to an extended structure.

The two boundary structures helix and antiparallel β-sheet respond 180° out of phase, which is usual for two species that are reversibly converted into each other. There are, however, three further modulation bands in the amide I′ region exhibiting phase angles, which are significantly different from those of the α- and β-structures and which are assigned to intermediate structures of poly-L-lysine (18).

Access to higher harmonics is a further powerful ability of modulation spectroscopy. In general, the response will reflect the same frequency ω as applied with a harmonic stimulation as given by Eq. (1). However, any nonlinearity on the signal path will result in higher harmonics. Excluding instrumental and optical nonlinearities, as admitted in this experiment, we may conclude that the detected 2ω response shown in Fig. 5C must result from a nonlinear chemical reaction scheme, i.e., a reaction scheme containing one or more reaction steps that differ from first order. A further interesting remark should be made: The temperature modulation amplitude $\Delta T_1 = 2°C$, which was applied in this experiment, is so small that only a weak perturbation of the stationary state should be expected. Under such conditions, higher-order kinetics reduce to first-order kinetics (8), producing responses only in the fundamental. The fact that this is not the case in practice, because of prominent 2ω responses, indicates that a magnification by the system must take place, which is typical for phase transitions.

Figure 5 shows the expanded amide I′ region of the stationary absorbance spectrum (A) and the parallel polarized modulation spectra in the fundamental frequency (ω) and the first harmonic (2ω). In the stationary spectrum (A), which represents the system at its mean temperature of 28°C, there are three clearly resolved bands, assigned to antiparallel pleated sheet (β-structure) at 1685 and 1614 cm^{-1}, respectively. The center band at 1639 cm^{-1} is assigned to the helix. At least four intermediate species may be localized by visual inspection of the

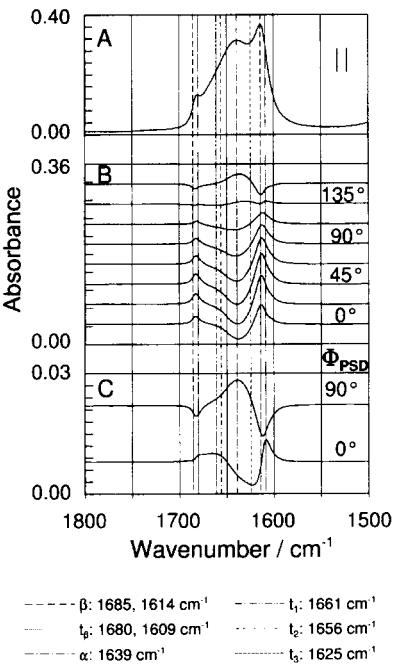

Fig. 5 Parallel polarized T-ME FT-IR spectra in the amide I′ region of a poly-L-lysine (PLL) deuterobromide film hydrated with D_2O (80% rel. hum., 28°C). Same experiment as described in the legend to Fig. 4. Expanded amide I′ region with (A) stationary absorbance spectrum, (B) 22.5° phase-resolved modulation spectra in the fundamental (ω), and (C) 90° phase-resolved modulation spectra in the first harmonic (2ω). In the stationary spectrum (A), which represents the system at its mean temperature of 28°C, there are three clearly resolved bands, assigned to antiparallel pleated sheet (β-structure) at 1685 and 1614 cm^{-1}, respectively, and the center band, which is generally assigned to a helix located at 1639 cm^{-1}. At least four intermediate species may be localized by visual inspection of the modulation spectra: Probably an intermediate antiparallel β-structure at 1680 and 1609 cm^{-1}, respectively, and three further components at about 1661, 1656, and 1625 cm^{-1}. The latter as well as the antiparallel β-structure have very prominent bands in the 2ω spectra (C).

modulation spectra: Most probable, an intermediate antiparallel β-structure at 1680 and 1609 cm^{-1}, respectively, and three further components at about 1661, 1656, and 1625 cm^{-1}. Nearly all modulation bands visible in spectrum B have corresponding bands in spectrum C. This means that a description of the folding process by first-order steps is most probably not correct, provided that the T-stimulation is free of a 2ω component, which was the case in this experiment. As a consequence, we have to assume second-order reactions or more compli-

cated steps due to cooperative phenomena. Second-order steps are surely involved, since PLL is dehydrated upon folding from helix- to β-structure. Finally, it should be noted that the antiparallel β-structure and the component at 1625 cm^{-1} have very prominent components in the 2ω spectra C, thus pointing to a distinct nonlinearity.

A detailed analysis based on T-ME experiments performed with different stimulation frequencies will be given elsewhere.

3.2 Concentration-Modulated Excitation (c-ME)

3.2.1 Experimental Considerations

The performance of a c-ME ATR experiment is based on a very simple concept. Two computer-controlled pumps are connected via a switch to the inlet of the flow-through cell. One pump is connected to a vessel containing solvent (e.g., a buffer solution) with a stimulant of concentration c_{0S}, whereas the other feeds solvent with stimulant concentration c_{0R}, where $c_{0S} > c_{0R}$ and $c_{0R} \geq 0$. During one half-period, c-ME is active due to pumping a high concentration of reactive compound through the cell, and in the following half-period relaxation occurs by pumping the low stimulant concentration. Under the condition of equal throughput in both channels, the stationary stimulant concentration becomes $(c_{0S} + c_{0R})/2$. This mean concentration should be adjusted in such a way that the system response is maximum to a change of stimulant concentration (maximum slope). Equation (12) now results in

$$c(t) = c_0 + \Delta c_0 + \Delta c_1 \cos(\omega t + \theta) = \underset{\uparrow}{\frac{c_{0S} + c_{0R}}{2}} + \Delta c_1 \cos(\omega t + \theta) \tag{16}$$

stationary state

While in the steady state, Δc_0 will be constant at any position in the flow-through cuvette; Δc_1 depends critically on hydrodynamic and diffusion parameters; and its range is $0 < \Delta c_1 \leq (c_{0S} - c_{0R})/2$. The ratio $2\Delta c_1/(c_{0S} - c_{0R})$ is referred to as *degree of modulation* ρ.

In order to achieve efficient c-ME, it is a prerequisite to take the convection/diffusion problem depicted in Fig. 6 into account. The upper part of Fig. 6 is a schematic vertical sectional view across the SBSR flow-through cell. Single-beam sample reference (SBSR) relates to a commercially available attachment converting a single-beam FT-IR spectrometer into a pseudo-double-beam spectrometer. In the ATR mode, the vertically aligned trapezoidal IRE is subdivided into an upper and lower half-plate, which can be used as reference and sample channel, respectively. Since the SBSR attachment converts the convergent IR beam of the spectrometer into a parallel beam of height h, sample (S) and refer-

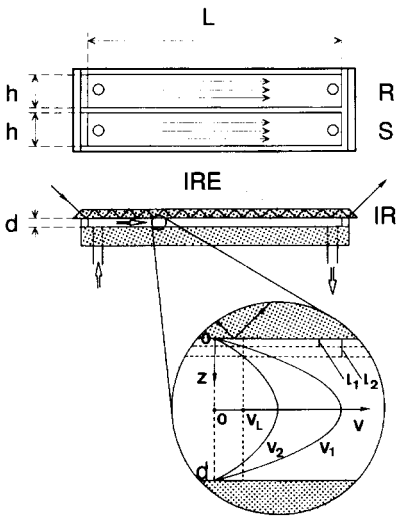

Fig. 6 Approximate description of the convection/diffusion problem encountered in the ATR flow-through cell. The liquid flow entering the cuvette at the left-hand side is assumed to be laminar in the cell. This results in a parabolic velocity profile $v(z)$, Eq. (17). As a consequence, the flow velocity v is zero at the boundaries $z = 0$ and $z = d$ (d: thickness of spacer S). Under these conditions, a stimulant molecule can reach the immobilized sample at the surface $z = 0$ of the internal reflection element (IRE) only by diffusion. On the other hand, the diffusion length l depends on the flow velocity v; i.e., the higher the velocity, the smaller the diffusion length l. The efficiency of concentration modulation depends critically on the dimensionless quantity $\omega \cdot l^2/D$, where ω and D denote angular frequency and diffusion coefficient, respectively; see Fig. 7.

ence (R) spectra can be scanned alternatively under computer control by moving the whole cell up and down. The main advantage of this technique is enhanced background compensation, which is prominent in the case of long-term measurements. Furthermore, water vapor and carbon dioxide compensation will no longer be a problem. For details the reader is referred to Refs. 5, 21, and 22.

The following assumptions have been made in order to get an approximate solution of the convection/diffusion problem: (a) Laminar flow in the cuvette: As a consequence, the flow rate at the IRE surface ($z = 0$) is zero; i.e., the transportation of the chemical stimulant to a sample immobilized at the IRE surface is not possible by convection but needs an ultimate diffusion step. (b) To make the coupled convection-diffusion problem analytically tractable, we assume a layer $0 \leq z \leq l$ within which diffusion only is considered. For $z > l$, diffusion is neglected; i.e., the stimulant is transported to the boundary $z = l$ by convection only.

It should be noted that unavoidable phase errors in the stimulation process

will occur when using a flow-through cell as depicted by Fig. 6, because excitation starts first in the region of the inlet and last at the outlet. The magnitude of this systematic error depends on the time t required to move the wavefront over the distance L, namely, $\Delta t(l) = L/v_L$. Where $v_L = v(l)$ denotes the laminar flow velocity at $z = l$. The inset in Fig. 6 illustrates the situation for two flow velocities $v_1 > v_2$. Consider a given velocity v_L at the outer diffusion boundary as marked by a dotted line perpendicular to the v-axis. In this example v_L can be reached by both velocities under consideration. However, one must be aware that the diffusion length becomes longer the slower the flow rate is; i.e., $l_2 > l_1$. Since, in general, diffusion is rate determining, one has to match the dimensions of the flow-through cell and the throughput of solution (i.e., the pumping rate) in order to get a desired response time of the cell and a good efficiency of c-ME.

Let us first consider the convection part. The laminar-flow velocity profile can be described by Eq. (17):

$$v(z) = \frac{6\dot{V}}{hd}\frac{z}{d}\left(1 - \frac{z}{d}\right) \tag{17}$$

$\dot{V}$ denotes the volume throughput (volume per time), and h, d, and z are height, thickness, and distance from the IRE, respectively, as depicted by Fig. 6.

The maximum velocity reached at $z = d/2$ and the mean flow velocity result, from Eq. (17), as

$$v_{max} = v\left(\frac{d}{2}\right) = \frac{3\dot{V}}{2hd} \quad \text{and} \quad \bar{v} = \frac{\dot{V}}{hd} \tag{18}$$

Now let us consider the diffusion process. The two boundary conditions required to solve the partial differential equation are $(\partial c/\partial z)(z = 0) = 0$ and Eq. (16) at $z = l$ with $\theta = -\pi/2$, which means excitation with a sine function. The initial condition is $c(z, t = 0) = 0$. The general stationary solution for the degree of modulation $\rho(z) = 2\Delta c_1(z)/(c_{0S} - c_{0R})$ is then given after solving the differential equation by

$$\rho(z) = \frac{\cosh\left[\kappa\frac{z}{l}(l + i)\right]}{\cosh[\kappa(l + i)]} \tag{19}$$

where

$$\kappa = \sqrt{\frac{\omega l^2}{2D}} = \sqrt{\omega_{red}} \tag{20}$$

ω is the angular frequency of ME, D is the diffusion coefficient, and l is the thickness of the diffusion layer. We refer to the dimensionless quantity ω_{red} as the reduced angular frequency, a quantity depending typically on the diffusion

parameters. Equation (19) is a complex function, indicating that an additive phase lag results from diffusion besides the amplitude damping. For our purpose the latter is of prime importance. One obtains, from Eq. (19),

$$\left|\rho\left(\frac{z}{l}\right)\right| = \sqrt{\frac{\cosh\left(\kappa\frac{z}{l}\right)^2 \cos\left(\kappa\frac{z}{l}\right)^2 + \sinh\left(\kappa\frac{z}{l}\right)^2 \sin\left(\kappa\frac{z}{l}\right)^2}{\cosh(\kappa)^2 \cos(\kappa)^2 + \sinh(\kappa)^2 \sin(\kappa)^2}} \tag{21}$$

Figure 7 presents the dependence of the degree of modulation $|\rho(z)|$ on the reduced angular frequency ω_{red} and the relative distance z/l from the IRE surface. The degree of modulation relevant for ATR experiments is obtained by the section parallel to the $\omega_{red}/|\rho(z)|$-plane at $z/l = 0$, i.e., at the surface of the IRE. It follows from Eq. (21) that

$$|\rho(0)| = \sqrt{\frac{1}{\cosh(\kappa)^2 \cos(\kappa)^2 + \sinh(\kappa)^2 \sin(\kappa)^2}} \tag{22}$$

It should be noted that in general the penetration depth d_p of the evanescent field (5,21,23) is small compared to the diffusion length l; the assumption $\rho(d_p) \approx \rho(0)$ is therefore a good approximation. The dependence of $\rho(z = 0)$ on the reduced frequency ω_{red} according to Eq. (22) must now be considered in order to design an efficient ATR flow-through cell for c-ME.

We are aiming to have a cell for c-ME studies with immobilized mono-

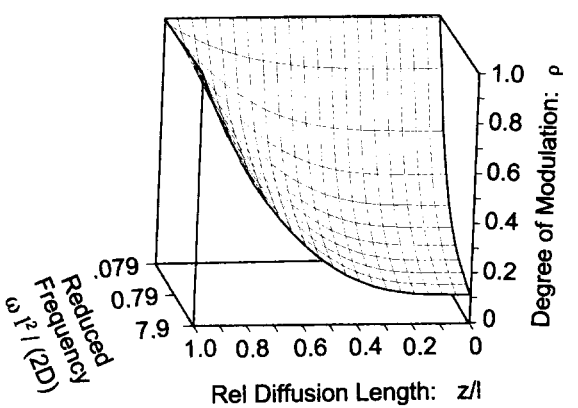

Fig. 7 Three-dimensional representation of the dependence of the degree of modulation $|\rho|$ on the dimensionless parameters relative diffusion length z/l and reduced frequency $\omega_{red} = \omega l^2/(2D)$ according to Eq. (21).

layers suited for a maximum frequency f_{max} = 0.1 Hz, which means that the stimulant is pumped during 5 s through the cell and washed out during the following 5 s, resulting in a stimulation period of τ = 10 s. Typical geometrical parameters of a flow-through cuvette adapted to c-ME are h = 7.5 mm, d = 0.1 mm, and L = 40 mm (22); see Fig. 6. The last is a principal requirement for an adequate number of internal reflections, when working with monolayers and submonolayers on a multiple IRE of thickness 1–2 mm (23).

Intending now to achieve a degree of modulation of $|\rho(0)|$ = 0.9 at the maximum frequency f_{max} = 0.1 Hz, we have to seek the required volume throughput $\dot{V}$. In order to get this information we first have to determine the diffusion length l required to achieve the conditions stated earlier. This problem can be solved numerically by means of Eq. (22) or graphically by means of Fig. 8.

Aiming for $|\rho(0)|$ = 0.9, it follows from Fig. 8 that $\log(\omega_{red}) = -0.23$, resulting in $l = 4.33 \cdot 10^{-2}$ mm for the diffusion length as calculated by means of Eq. (20). The next step in our evaluation is to decide on the maximum systematic phase error $\Delta\theta_{max}$ acceptable in the stimulation process. Setting $\Delta\theta_{max} = 2\pi(\Delta t_{max}/\tau) = \Delta t_{max} \cdot \omega_{max} = 0.314$, which corresponds to 5%, where τ means the duration of a ME cycle. According to our initial assumptions we have $\omega_{max} = 2\pi f_{max} = 0.628$, resulting in $\Delta t_{max} = 0.5$ s for the maximum time allowed to the wavefront to pass at distance $z = l$ along the length L of the cuvette. The

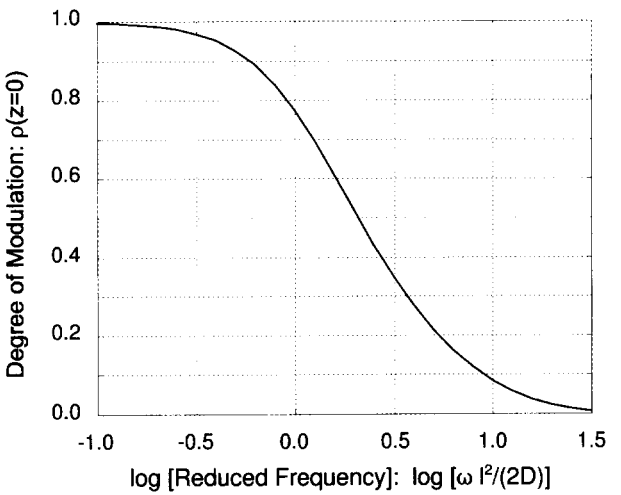

Fig. 8 Dependence of the degree of modulation $|\rho(0)|$ at the surface of the internal reflection element (IRE) as a function of the reduced frequency $\omega_{red} = \omega l^2/(2D)$ according to Eq. (22).

corresponding minimum velocity is $v_{min}(l) = L/\Delta t_{max} = 8.0$ cm/s. In order to get the corresponding volume throughput, one has to solve Eq. (17) for $\dot{V}$, resulting in

$$\dot{V} = \frac{v_{min}(l)hd^2}{6l\left(1 - \frac{l}{d}\right)} \tag{23}$$

Inserting the values from earlier into Eq. (23) one obtains, for the volume throughput, $\dot{V}(d = 100\ \mu m) = 2.44\ cm^3/min$. For comparison, enhancing the cell thickness to $d = 200\ \mu m$ would require enhancement of the volume throughput to $\dot{V}(d = 200\ \mu m) = 11.3\ cm^3/min$, which demonstrates that cell thickness is a critical parameter. Although this evaluation is approximate, it has proven to be reasonable in practice.

3.2.2 Influence of Ca^{2+} Ions on Structure and Activity of Acetylcholinesterase (AChE)

Little is yet known about structure–activity relationships of proteins and receptors under in situ conditions. ATR c-ME experiments are possible means to get such information on a molecular level. The activity of the enzyme acetylcholinesterase (AChE) is known to depend critically on the concentration of Ca^{2+} (24,25). Thus Ca^{2+}-c-ME may be used to get structural details related to the periodic change of AChE activity. The result is shown in Fig. 9.

AChE isolated from *Torpedo marmorata* was immobilized as monolayer at the surface of a germanium (Ge) IRE by adsorption to an aminopropyl triethoxysilane (ATS) layer (26). The activity of the enzyme was determined by means of the Ellman method, the surface concentration of the enzyme was determined spectroscopically (5,21,23). As a consequence, the IR-ATR technique enables in situ measurement of structure and activity. It should be noted at this point, however, that the main problem encountered with experiments of this type is not primarily a technical one, provided high-performance equipment is used, but rather a biochemical one, namely, the preparation of stable immobilized systems. Furthermore, in the context with in situ activity measurements, the adsorption of the enzyme in the tubes and on the rear cover of the flow-through cuvette must also be taken into account.

Figure 9 shows the amide I/II range of the stationary single-channel spectra I and I_0, the corresponding transmittance $T = I/I_0$ and the parallel polarized c-ME spectrum in absorbance units. The experiment was performed in H_2O buffer, pH 7.0, 0.1 M NaCl. The Ca^{2+} concentrations for stimulation and relaxation were $c_{0S} = 1.25$ mM and $c_{0R} = 0.25$ mM, respectively. Modulation bands with positive sign are typical for high Ca^{2+} concentration; negative bands reflect the AChE response to low Ca^{2+} concentration, i.e., reduced activity. The typical bands for enhanced activity are located at 1652 and 1677 cm^{-1}, whereas reduced activity

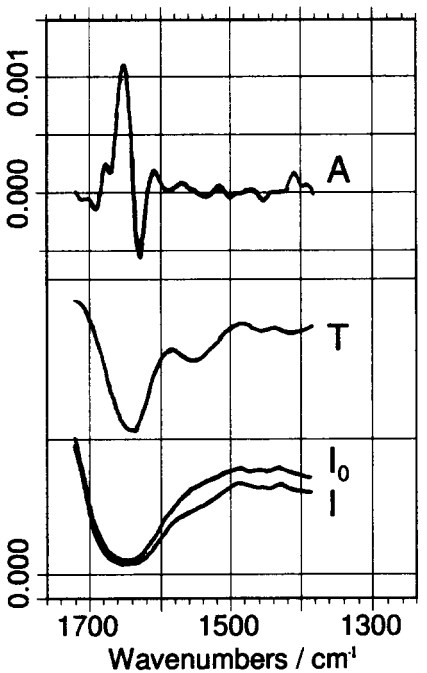

Fig. 9 AChE monolayer adsorbed to a Ge IRE pretreated by aminopropyl triethoxysilane. Parallel polarized Ca^{2+}-c-ME spectrum with Δc_0 = 0.75 mM and Δc_1 = 0.5 mM (see Eq. (16)). 0.1 M NaCl, pH 7. The resulting modulation of the specific activity was found to be (650 ± 150) IU/mg. Frequency f = 0.1 Hz. Ge IRE, 38 active internal reflections, angle of incidence Θ = 45°. (Reproduced from Ref. 25 by permission of Photo-Optical Instrumentation Engineers.)

is expressed by three resolved bands at 1630, 1665, and 1690 cm^{-1}. Since the process of c-ME is cyclic, distinct positive and negative bands must correspond to each other. The most probable combination is 1652 cm^{-1} with the couple at 1630 and 1690 cm^{-1}. The former is typical for a helix or random coil, while the latter reflects an antiparallel pleated sheet structure. The couple 1665/1677 cm^{-1} remains, which probably results from intermediate states with β-turns involved.

This finding is consistent with pH modulation experiments, which also lead to a periodic alteration of the enzyme activity (25). Finally it should be noted that only 0.5–1% of the amino acids of AChE were involved in the dynamic changes reflected by the modulation spectrum. Therefore one may conclude that activity control in an enzyme takes place by very small folding/unfolding processes.

3.2.3 Influence of the Degree of Protonation on the Structure of an Arachidic Acid (ArAc) Bilayer

The aim of this study was to get information on the influence of electrical surface charges on the molecular structure of an immobilized arachidic acid bilayer, which may be considered as a rough model of the lipid bilayer frame of a biomembrane. For that purpose, two monolayers have been transferred at a constant pressure of 25 mN/m from the air/water interface of a film balance to the Ge IRE by means of the Langmuir–Blodgett (LB) technique. Since the surface of Ge is hydrophilic, the first layer attached by its polar heads, whereas the second layer attached tail-to-tail. As a consequence, the carboxylic acid groups of the second layer faced the aqueous environment and were therefore accessible for protons or hydroxyl ions. A periodic pH modulation between pH 3 and pH 10 was used to induce a periodic protonation and deprotonation of the carboxylic acid groups. It should be noted that the binding of the ArAc head groups to the Ge surface was so unusual that typically very intense absorption bands of the carboxylic acid group, such as C=O stretching, were completely erased in the spectrum of the inner layer. Therefore, one may assume that the head group signals shown in Fig. 10 result predominately from the second monolayer of ArAc facing the electrolyte.

3.2.3.1 Assignment of Prominent Bands

Most assignments given next relate to Ref. 27. The upper traces in Fig. 10A and B show the stationary polarized ATR spectra A_0 of the ArAc bilayer in the protonated state. They are scaled down for comparison with the modulation spectra. The intense band near 1700 cm^{-1} results from C=O stretching of the COOH group. It consists of at least two components as reflected by the perpendicular polarized spectrum, Fig. 10B. Splitting into two components is also observed with $\nu_{as}(COO^-)$ near 1570 cm^{-1} and $\nu_s(COO^-)$ near 1430 cm^{-1}. So far it has not been established whether this splitting is typical for the bilayer or whether it is due to local crystallization phenomena (28,29). The narrow peak at 1470 cm^{-1} is assigned to the methylene bending vibration $\delta(CH_2)$, and the shoulder at 1460 cm^{-1} results most probably from the out-of-phase deformation of the methyl group $\delta_{as}(CH_3)$. The weak and broad band at 1407 cm^{-1} may be assigned to in-plane COH deformation of the COOH group and the symmetric methyl bending $\delta_s(CH_3)$. Finally, there is a sequence of nearly equidistant weak bands between 1180 cm^{-1} and 1350 cm^{-1} resulting from the wagging vibrations $\gamma_w(CH_2)$ of the methylene groups of hydrocarbon chains. This sequence originates from vibrational coupling in a saturated hydrocarbon chain assuming all-trans conformation. If N denotes the number of CH_2 groups of the chain, the selection rule predicts $N/2$ IR active vibrations for N even (symmetry C_{2h}). For N odd, all the wagging vibrations are expected to be IR active, $1/2(N - 1)$ are perpendicular

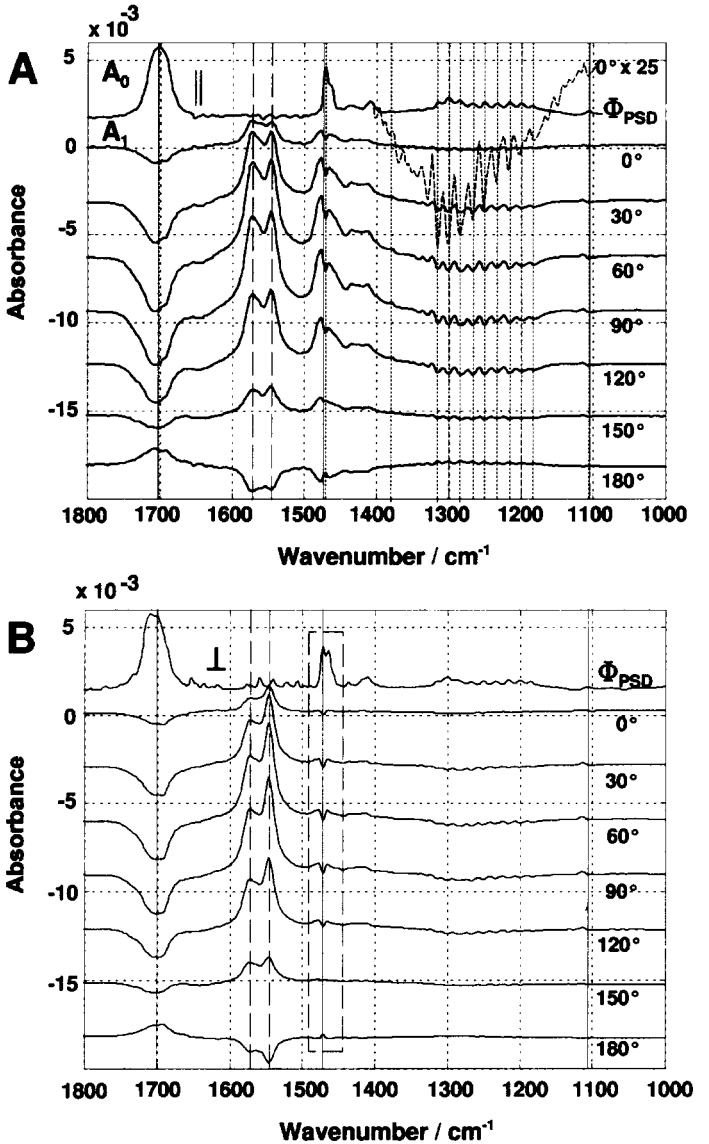

Fig. 10 pH-modulated excitation (ME) of an arachidic acid (ArAc) bilayer attached to a germanium internal reflection element (IRE). c-ME was performed by pumping alternatively two buffer solutions (100 mM NaCl, pH 3, and 100 mM NaCl, pH 10) through the ATR cuvette with a modulation period of $\tau = 16$ min, $T = 10°C$. Upper trace A_0: Stationary spectrum of a protonated ArAc layer for comparison with modulation spectra. Traces A_i: Modulation spectra at PSD phase settings $\phi_{PSD} = 0°, 30°, \ldots, 180°$. The 180° spectrum

polarized (very weak) and $1/2(N + 1)$ are polarized parallel to the symmetry plane (30). A prerequisite for vibrational coupling is all-trans conformation. Therefore, coupling is interrupted by any gauche defect, resulting in shorter all-trans segments with corresponding wagging bands at different wavenumbers. As a consequence, an increasing number of gauche defects at different chain positions will erase the well-resolved wagging sequence due to overlapping and loss of intensity. Finally, the weak band at 1104 cm^{-1} is assigned to C—C stretching ν(C—C).

3.2.3.2 Sensitivity of Modulated Excitation Spectroscopy

Taking the pH-modulation spectra shown in Fig. 10 as a typical example, one may check the sensitivity by expanding the lowest intense ME spectrum ($\phi_{PSD} = 0°$) by a factor of 25. The result is shown as the inset in Fig. 10A (top). The wavenumbers of the wagging peaks of the expanded spectrum still coincide with those of the most intense ME spectra ($\phi_{PSD} = 60°$ and $\phi_{PSD} = 90°$; the maximum is expected at $\phi_{PSD} \approx 75°$; so $\phi_{PSD} \approx 165°$ should result in an intensity of zero) and with the stationary spectrum A_0. The ordinate scaling factor for the zoomed inset is $4.0 \cdot 10^{-5}$. Comparing it with the other ME spectra (scaling factor $1.0 \cdot 10^{-3}$) one can conclude that bands as weak as $1.0 \cdot 10^{-5}$ absorbance units are still detectable.

Finally, it should be noted that this experiment has been performed in liquid H_2O. As a consequence, there was very low spectral energy in the 1640-cm^{-1} region. Nevertheless, a high-quality background compensation is achieved due to the application of modulation technique.

3.2.3.3 Selectivity of pH-ME

The highest selectivity of ME spectroscopy is achieved when the stimulation frequency ω and the kinetics of the stimulated process are matched, i.e., if $0.1 < \omega \cdot \tau_i < 10$, where τ_i denotes the ith relaxation time of the system. In the actual case of pH modulation exerted to the outer monolayer of ArAc, there is no phase resolution achieved, due to the long modulation period of $\tau = 16$ min; therefore no kinetic information is available from these measurements. However, unambiguous discrimination between protonated and deprotonated populations is possible. Only one characteristic example shall be given here. The most promi-

---

corresponds to the 0°-spectrum with opposite sign, because the PSD output is proportional to $\cos(\varphi - \phi_{PSD})$; see Sec. 5. φ denotes the phase difference between the response of a distinct part of the molecule and the stimulation. Due to the long period of $\tau_m = 16$ min, the observed bands in the modulation spectra exhibit only two resolved φ-values, which are 180° apart, as a consequence of the fact that the chemical relaxation time of protonation/deprotonation of ArAc is much shorter than the stimulation period. In order to demonstrate the excellent S/N ratio, the ordinate of the weakest modulation spectrum has been expanded in the CH_2-wagging region by a factor of 25, i.e., the ordinate scaling factor on top of the spectrum results in $4.0 \cdot 10^{-5}$ for the dashed spectrum.

nent band from the protonated state is the C=O stretching vibration ν(COOH) of the carboxylic acid group near 1700 cm^{-1}. Thus all other bands in the ME spectrum that have the same phase belong to the protonated population; they are considered to be correlated. The remaining bands featuring opposite sign are therefore members of the deprotonated population. Consequently, if no phase resolution is achieved, ME spectra reduce to difference spectra, which, however, have a considerably better background and instability compensation than conventional difference spectra, since corresponding sample and reference spectra are measured and evaluated/accumulated within each period τ of stimulation.

3.2.3.4 Spectroscopic Features

Concerning the application of ATR spectroscopy to biomembranes, the reader is referred to Refs. 5, 21, and 23. Let us now consider the wagging region $\gamma_w(CH_2)$ of the spectra shown in Figs. 10A and B. In the stationary absorbance spectrum A_0, one can observe nine weak bands resulting from the 18 CH_2 groups of the ArAc molecules. We can conclude that the majority of the hydrocarbon chains assume all-trans conformation. Moreover, the wagging sequence in the parallel polarized spectra is significantly more intense than the spectra measured with perpendicular polarized light. This means that hydrocarbon chains are aligned toward the normal of the IRE. This experimental finding is even more prominent in the modulation spectra, which shall be considered now. We look for bands exhibiting the same phase behavior. They represent a population of molecules or parts of them that are correlated, i.e., respond in the same way to the external stimulation. In this experiment the kinetic response to pH change was much faster than the stimulation period of $\tau = 16$ min. Therefore, we have only the protonated and the deprotonated population with phase angles 180° apart. In order to identify a population, it is sufficient to have a reliable assignment of one its bands. Taking, e.g., the modulation spectrum with $\phi_{PSD} = 90°$, we can group the bands into positive and negative ones. Since the band at 1700 cm^{-1} is negative, we know unambiguously that all negative bands of this spectrum belong to the population of protonated ArAc. Consequently, all positive bands at this PSD phase setting belong to the population of the deprotonated ArAc. We can therefore conclude that both $\delta(CH_2)$ and $\gamma_w(CH_2)$ decrease and that ν(C—C) shifts as ArAc is deprotonated. The population of deprotonated ArAc appears with 180° phase difference. Besides the split $\nu(COO^-)$ bands already mentioned, attention must be drawn to a very strange phenomenon, which probably reflects an electric field effect originating in the negative surface charge density at the planar membrane surface, which is produced by deprotonation. At 1470 cm^{-1} we recognize the sharp vanishing $\delta(CH_2)$ band that is overlapped by an intense and broad positive band. Moreover, this band, which belongs unambiguously to the population of deprotonated ArAc, is completely parallel polarized. The only explanation of this fact is alignment of the transition dipole moment of this band parallel to the normal to the IRE, i.e., parallel to the electric field. We assign this band tenta-

tively to a $\delta(CH_2)$ vibration disturbed by the strong electric field. A more detailed discussion of this phenomenon that also takes into account the behavior of CH-stretching will be given elsewhere (D. Baurecht, G. Reiter, M. Schwarzott, U.P. Fringeli. J Phys Chem, in preparation).

3.3 Electric Field–Modulated Excitation (E-ME)

Very strong electric fields are expected in biomembranes, at least in certain regions. The magnitude may be estimated from the knowledge that the transmembrane potential is about 100 mV and the membrane thickness about 100 Å thus resulting in an electric field in the order of magnitude of 10^7 V/m. Nature uses such high electric field strengths for process control, which means that a coupling to biochemical reactions must occur. Understanding of these reaction mechanisms are therefore of fundamental interest.

So far, considerable theoretical knowledge exists on electric field/biomembrane interaction (31), but only few experimental data are available. The reason is evident, since exposing a biological model system to such extremely high electric field strengths is not an easy operation. However, it is a challenge to try to simulate membrane electrostatic conditions in order to study the response of model compounds on a molecular level.

Indeed, there are several possibilities for exposing model membranes to electric fields of comparable strength. One approach is the direct application of electric potentials across the membrane using a Ge IRE and the rear cover of the cuvette as electrode and counter electrode, respectively. The main problem encountered with this setup is electrochemical degradation of the Ge IRE surface, leading to reduced transmittance and, more critically, to the liberation of protons due to the formation of germanic acid (H_2GeO_3) when the Ge IRE is held on a positive potential (32). Experiments of this type may be performed with a hydrated sample sandwiched between two narrowly spaced electrodes. This setup has turned out to require sealed cuvettes and surface-coating-protected Ge IREs.

An indirect method to apply a strong electric field has already been presented in the preceding section—by controlling the surface charge density of a membrane via the pH, whereas a second indirect method makes use of the very strong electric fields occurring in the electric double layer at an electrode surface. The space charge of the double layer can easily and quickly be influenced by very low electrode potentials. However, only very thin immobilized layers can be exposed to these fields, because the penetration depth of the space charge region into the electrolyte is very small. Depending on the ionic strength of the electrolyte, it varies between a few and several hundred angstroms.

It should be noted that the experiments discussed next are preliminary. Nevertheless they deserve to be mentioned, because unambiguous evidence is given that E-ME is feasible and enables a promising approach to get more insight into membrane electrostatics.

3.3.1 Direct Application of High Potentials to Hydrated Lipid Multibilayers

In order to study the influence of electric fields to multibilayers of 1,2-dimyristoyl-sn-glycero-3-phosphocholine (DMPC) by IR-ATR spectroscopy, the Ge IRE and the Ge counter electrode were protected by a SiO_2 coating. Multibilayers of DMPC were prepared on the IRE simply by evaporation of the organic solvent of a dilute DMPC solution. The IRE and the counterelectrode were separated by a 5-μm spacer. The lipid was hydrated before sealing of the cell. Potentials up to 200 V could be applied across the lipid phase, resulting in conformational and reorientational effects. The surface coating of the Ge plates was necessary to prevent electrical discharge at elevated electric potentials. Measurements of E-ME using this setup are in progress (personal communication: P. Lasch, D. Naumann, Robert Koch Institute, Berlin).

3.3.2 Indirect Application of Modulated High Potentials to an Immobilized Poly-L-lysine Layer

The experimental setup is schematically depicted in Fig. 11. The Ge IRE and the stainless steel rear cover act as electrodes. The latter is grounded, while the former assumes a rectangular potential switched between +50 mV and −1000 mV. Working within these potentials avoids, on the one hand, anodic hydrolysis of Ge (32) and, on the other hand, hydrolysis of water. The modulation period was $\tau = 20$ min. Changing the polarity of the potential at the IRE leads to an

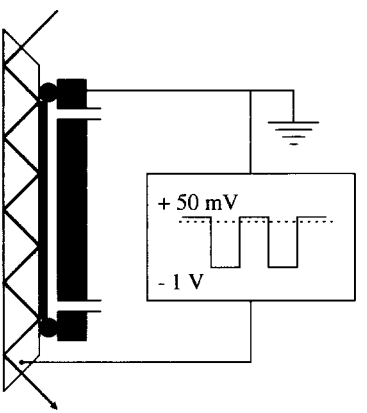

Fig. 11 Schematic view of a setup for electric field–modulated excitation (E-ME). The sample is immobilized as thin film on the surface of the Ge IRE, which acts as one electrode. The grounded counterelectrode is the rear stainless steel cover of the cuvette, which is filled with electrolyte solution. Stimulation is performed by applying a rectangular potential varying between +50 mV and −1000 mV. These potentials are selected to avoid degradation of Ge at higher positive potentials as well as to avoid electrolytic decomposition of water.

exchange of the ions in the space charge region of the electric double layer at the membrane surface. If the ionic strength is kept low, e.g., about 1 mM as in this case, the Debye length, which determines the thickness of the space charge region, will be in the order of 100 Å. As a consequence, very high electric fields are switched at the surface of the electrode upon changing the polarity (33). Consequently, a thin immobilized layer, such as a model membrane or a protein layer, will be exposed to high electric fields, too. This indirect method may be used to study the influence of an alternating high electric field on a poly-L-lysine (PLL) film immobilized by adsorption to the surface of the Ge IRE (34).

Preliminary results are shown in Figs. 12 and 13. It should be noted that a rectangular ME, as applied in this case, besides the fundamental frequency ω (1), also results in all odd harmonics, i.e. 3ω, 5ω, . . . , but with decreasing intensity. However, there is no excitation with even multiples of the fundamental. Therefore, detection of even spectral responses is of special interest, since those result from frequency doubling by the stimulated system, provided the modulated

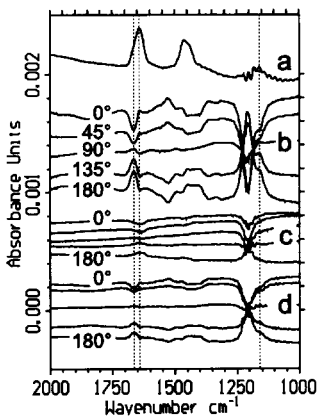

Fig. 12 E-ME of a poly-L-lysine (PLL) film adsorbed to a Ge IRE in contact with liquid D_2O, pD = 10. Exposure of PLL to high electric fields was performed indirectly via the exchange of the space charge in the electric double layer by applying a periodic rectangular potential varying between +50 mV and −1000 mV. Parallel polarized incident light, angle of incidence $\Theta = 45°$, $N = 19$ active internal reflections, $T = 30°C$. (a) Stationary spectrum, (b) phase-resolved modulation spectra obtained by sinusoidal demodulation with the fundamental frequency ω. (c) Phase-resolved modulation spectra obtained by sinusoidal demodulation with the first harmonic frequency 2ω. Note that this frequency is not included in a rectangular stimulation with frequency ω. Frequency doubling has occurred by the response of PLL. See also expanded section in Fig. 13. (d) Phase-resolved modulation spectra obtained by sinusoidal demodulation with the second overtone frequency 3ω. Note: This response is again initiated by the stimulation, since a symmetric rectangular wave contains all odd multiples of the fundamental. The intensity is damped by the factor $1/(2n + 1)$, with $n = 0, 1, 2, \ldots$. For details see text.

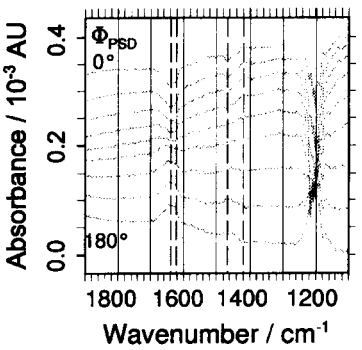

Fig. 13 Expanded section of the 2ω response modulation spectra shown in Fig. 12(c). Same data but enhanced phase resolution of $\Delta\phi_{PSD} = 22.5°$. Three amide I′ components are resolved, namely, at 1639 cm^{-1}, 1620 cm^{-1}, and about 1600 cm^{-1}. The first two bands overlap; however, the change in shape with varying ϕ_{PSD} indicates a slight difference in the response phase angle. Corresponding modulation bands are detected in the amide II′ region, too. Most probably the band at 1470 cm^{-1} correlates with the amide I′ component at 1639 cm^{-1} and may be assigned to helix (18). A further correlation exists between the amide I′ and amide II′ components at 1600 cm^{-1} and 1420 cm^{-1}. These two populations are 180° out of phase; i.e. they are periodically converted into each other.

system response is small so that the signal transfer remains linear. In this case, the small signal condition is surely fulfilled, as can be verified from absorbance scaling of Figs. 12 and 13.

Figure 12 presents the downscaled parallel polarized stationary spectrum of the PLL film (a) in liquid D_2O environment. Three resolved bands are observed, namely, the amide I′ band near 1639 cm^{-1}, the amide II′ band near 1450 cm^{-1}, and the band near 1160 cm^{-1}, which we assign to the—ND_3^+ antisymmetric bending of the lysine side chain. The noise in this region results form low energy due to strong D_2O absorption [$\delta(D_2O)$ at 1200 cm^{-1}]. The dotted vertical lines indicate $\delta_{as}(ND_3)$, helix at 1639 cm^{-1}, and a component at about 1665 cm^{-1}, which was also observed as intermediate species in T-ME experiments with PLL (see Sec 3.1). No unambiguous assignment of this band is available so far. Traces (b)--(d) of Fig. 12 are modulation spectra with indicated PSD settings (see also Sec. 5). Part (b) represents the PLL response to the excitation with the fundamental ω, while (d) is the response to the 3ω excitation. According to the Fourier series of a symmetric rectangle, the intensity of the 3ω component should be reduced by a factor of 1/3 with respect to the fundamental, which is approximately the case. Spectrum (c) is the 2ω response of PLL to rectangular E-ME. Since no 2ω component exists in the stimulation and all signal amplitudes are very small, which guarantees a linear signal transfer, we can conclude that the

weak but significant band at 1639 cm^{-1} has a different origin than the other modulation bands. The signal-to-noise ratio of this measurement is good enough to expand the 1800–1200-cm^{-1} region of Fig. 12(c). This region is shown with enhanced phase resolution of $\Delta\phi_{PSD} = 22.5°$ in Fig. 13. Comparing the shape of the amide I′ band along the PSD phase settings, we realize that the shapes are not similar in a mathematical sense; i.e., they cannot be converted into each other by simple multiplication with an adequate factor. Therefore, we have to conclude that at least two components overlap in this band. Visual inspection indicates components at 1639 cm^{-1} and 1620 cm^{-1}. Moreover, these two components seem to have a slightly different phase response, which is responsible for the nonsimilarity of the band shapes. At $\phi_{PSD} = 0°$ they are close to their minima (negative bands). A weaker, third band with opposite sign is observed at about 1600 cm^{-1}. It vanishes and changes sign at about the same PSD phase setting of $\phi_{PSD} = 90°$; i.e., 1639/1620-cm^{-1} and 1600-cm^{-1} bands have a phase difference of about 180°. A corresponding behavior is also observed in the amide II′ region. The bands at about 1470 cm^{-1} and 1639 cm^{-1} are correlated. They have been assigned earlier to the α-helical part of PLL (18). On the other hand, the band at about 1420 cm^{-1} correlates with the 1600 cm^{-1} band. For both, there is no reliable interpretation available at present. Additional measurements at elevated excitation frequencies in order to achieve significant time resolution are necessary to get better experimental discrimination.

Concerning the origin of the 2ω response, a definite answer also cannot be given at present. According to Eqs. 10 and 11, the influence of the electric field on a rate constant via field/induced dipole interaction or spacial reorientation of PLL segments by field/permanent dipole interaction are both possible explanations.

Coming back to the ω and 3ω responses shown in Fig. 12, traces (b) and (d). In the amide I′ region there is a well-resolved reversible conversion between 1665 cm^{-1} and 1639 cm^{-1}. Both bands are known from T-ME experiments (see Sec. 3.1 and Ref. 18). The latter is assigned to the helix; the former probably represents β-turns. Quite obviously, the rate constant of this conversion seems to be considerably more sensitive to electric fields than rate constants associated with other folding steps occurring in the PLL chain. According to Eq. 10, one may assume a high permanent reaction dipole moment between the initial state and the transition state of this elementary reaction. Therefore, it seems a likely supposition that folding or unfolding of α-helical segments is involved in this step.

Let us consider the spectral region around 1200 cm^{-1}. The D_2O bending vibration at 1200 cm^{-1} is very well compensated in the stationary spectrum of Fig. 12(a), but it is present in all the modulation spectra of Fig. 12(b)–(d). This means that water molecules are also involved in the cyclic process induced by E-ME. The phase of the $\delta(D_2O)$ modulation band correlates with the 1665-cm^{-1} band. A possible interpretation is a change of hydration of PLL during the 1639/

1665-cm^{-1} transition. However, there might also result significant contributions from cyclic exchange of hydrated anions and cations in the space charge region.

A second band in this region should be mentioned, namely, the antisymmetric bending vibration of ND_3^+, $\delta_{as}(ND_3)^+$ at 1160 cm^{-1}. It appears only in the ω and 3ω spectra and correlates with the 1665-cm^{-1} band. Whether the 1639/1665-cm^{-1} reaction step involves a deuteronation of the ε amino group of the lysine side chain will be the subject of further investigations.

Finally, it should be mentioned that the uneven trace of the ω and 3ω modulation spectra in the region between 1550 cm^{-1} and 1250 cm^{-1} is not understood up to now. There is no signal-to-noise problem, since the bands exhibit a systematic behavior with respect to the PSD phase setting and, moreover, they correlate in part with the 1665-cm^{-1} and with the 1639-cm^{-1} bands, respectively.

3.4 UV-VIS–Modulated Excitation (Φ-ME)

UV-VIS–modulated excitation (Φ-ME) IR spectroscopy could be of significant importance in the investigation of photochemical processes in biology, biochemistry, and chemistry. To our knowledge, no biochemical/biological applications of Φ-ME have been reported so far. Therefore, an example of a sophisticated and pioneering study of the photo-oxidation of pyrocatechol by Φ-ME IR will be presented in short. In this study, Φ-ME IR was supported by complementary Φ-ME ESR experiments, which were very useful for the identification of photochemically produced radicals. For details the reader is referred to Ref. 9.

Pyrocatechol (I, in Fig. 15) was dissolved in carbon tetrachloride with a concentration of $4.0 \cdot 10^{-4}$ mol/L. A transmission flow-through cell of 10-cm path length was used for IR spectroscopy. One side wall of the cell consisted of a quartz window, enabling UV irradiation of the solution. Ultraviolet light from a xenon lamp was interrupted by a mechanical chopper in the frequency range of 2–100 Hz. The IR beam transmitted the cuvette at a right angle to the UV beam. The periodic response of photoexcited species were demodulated by phase-sensitive detection (PSD; see also Sec. 5). The components of the modulation spectra obtained with PSD phase settings 0° and 90° with respect to the excitation were separated in the spectral region of 3200–3700 cm^{-1} by lineshape analysis. This procedure enabled optimum accuracy for the determination of amplitude/frequency and phase/frequency relations. The results of this analysis are presented as Bode diagrams in Fig. 14, which together with a theoretical kinetic analysis formed the basis for the determination of the reaction scheme shown in Fig. 15 as well as of the corresponding rate constants, which were determined by fitting the Bode diagrams. Some interesting key aspects should be mentioned, because they were essential for the postulation of the reaction scheme shown in Fig. 15. From stationary irradiation experiments three end products (III, IV, V) were known. Furthermore, kinetic analysis of the reversible cycle formed by the

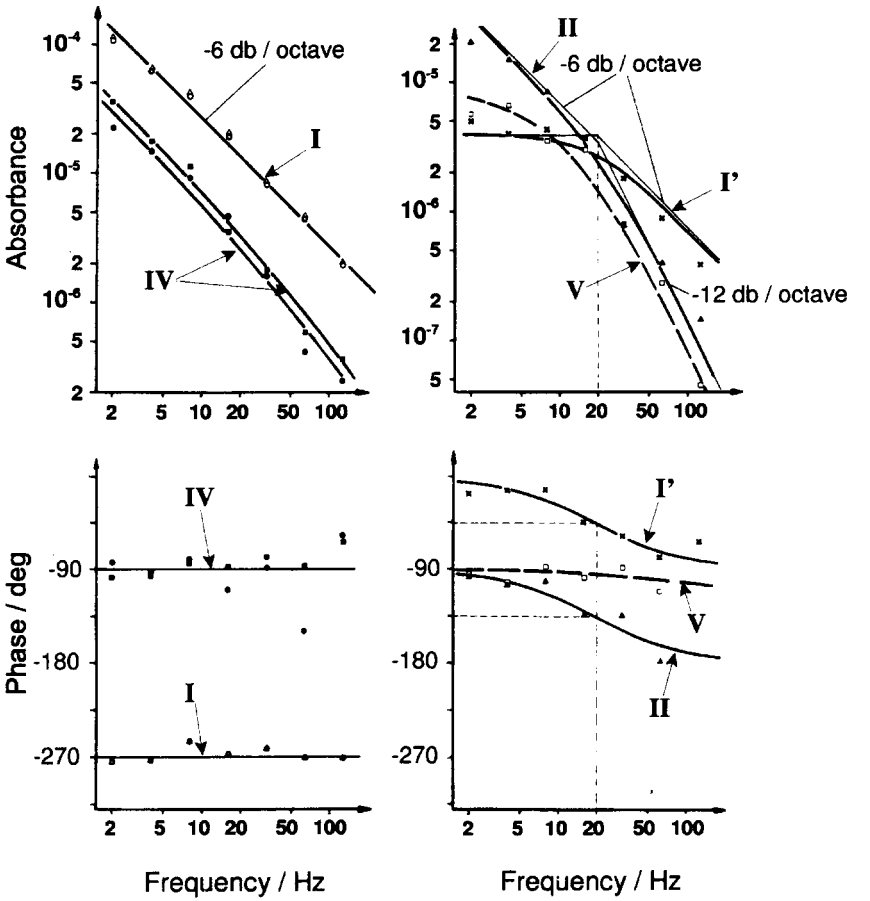

Fig. 14 Bode diagrams in the frequency range 2–100 Hz from Φ-ME IR absorption bands of pyrocatechol in carbon tetrachloride solution ($4.0 \cdot 10^{-4}$ mol/L, 295 K, N_2 purging). The Roman numbers indicate the species and the corresponding frequencies of the modulation bands as indicated in the reaction scheme Fig. 15. (Reproduced from Ref. 9 by permission of North Holland Publishing Company.)

ground state S_0 (I), the singlet excited state S_1, and the triplet state T_1 (see Fig. 15) with slow, irreversible exits resulted in the following finding (9): At low frequencies, ground state I exhibits a phase shift of $-270°$ with respect to the stimulation. Its frequency dependence is a −6-decibels (dB) decrease per octave at elevated frequencies. Excited singlet and triplet states are too short-lived to achieve detectable concentrations. Under the condition of a short-lived S_1, the

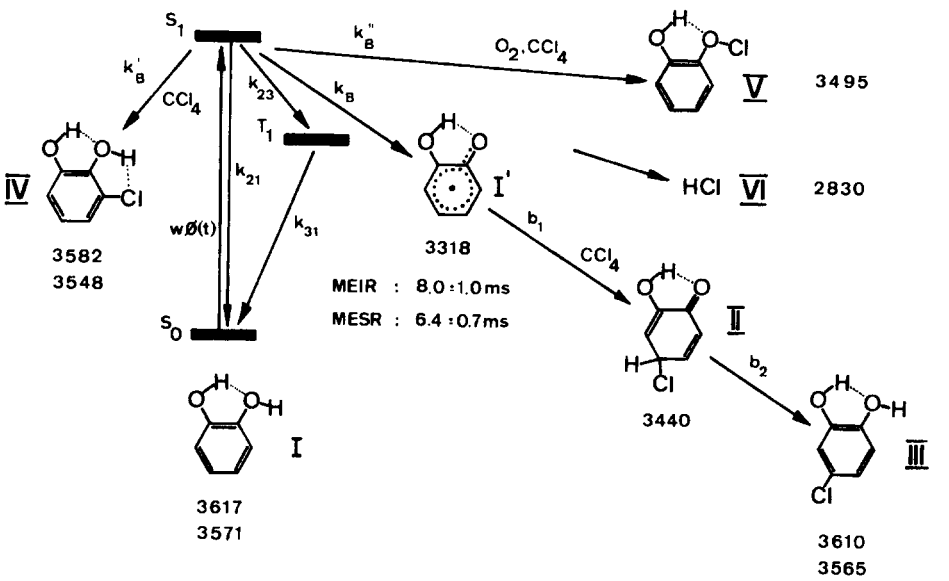

Fig. 15 Kinetic scheme of the photo-oxidation of pyrocatechol in carbon tetrachloride as determined by Φ-ME IR and Φ-ME ESR spectroscopy. (Reproduced from Ref. 9 by permission of North Holland Publishing Company.)

first particle in an irreversible exit chain of only first-order reactions will exhibit a phase between 0° and −90° as the frequency is increased from zero to infinity. The amplitude decrease at high frequencies is −6 dB/octave. For each succeeding compound in this chain, one has to add −90° to the phase and an additional −6-dB/octave to the slope of the log (amplitude) vs. log (frequency) plot at elevated frequency. However, a second-order reaction step will result in a steeper slope even by itself, e.g., −12 dB/octave as observed with particle V.

In practice, the bode diagrams shown in Fig. 14 have been determined from the experimental results. Three irreversible paths were found: Particles I′ and II behave as first and second compound in a linear chain with first-order kinetics. Particle IV also behaves like the first compound in a chain with first-order reactions. Consequently it must be on a second exit from S_1. In addition, it was found independently to be an end product. From the amplitude/frequency behavior, particle V behaves similarly to particle II, which is on the second place in the chain of irreversible first-order reactions. Consequently, particle V must be on a third irreversible exit from S_1. Independently it was found that production of particle V depends on the oxygen content of the solution. Therefore it is most probable that the end product V is formed directly from S_1 by a second-order

reaction. Finally, the OH stretching bands of pyrocatechol (I) could also be assigned due to the phase/frequency behavior, which at low frequency should result in a phase angle of $-270°$.

4 TWO-DIMENSIONAL CORRELATION ANALYSIS

Absorption bands of modulation spectra that exhibit equal phase shifts with respect to the external stimulation are considered to be correlated. Two-dimensional correlation analysis is a statistical/graphical means to visualize such a correlation in a 2D plot, which was referred to as a 2D IR spectrum (4). For theoretical background, the reader is referred to Refs. 4 and 18. In general, correlation analysis is made between two modulation spectra with PSD settings 90° degrees apart from each other. However, correlation between any difference of PSD phase settings may be calculated and obviously can lead to a more accurate estimation of the relative phase shift between two bands. Since 2D IR spectra are very susceptible to noise, it was shown that introducing a threshold and plotting only 2D signals above this limit may help disentangling the correlation data (18).

In any case, one may have a different opinion about the scientific value of 2D spectroscopy applied to data obtained via ME. In order to enable the reader to form his own opinion, a synchronous 2D IR spectrum was calculated from the 0° and 90° modulation spectra of Fig. 10A and is presented in Fig. 16. Two interesting features of 2D IR spectroscopy should be mentioned. First, the intensity of cross-peaks is proportional to the product of the intensities of the two bands under consideration. Consequently, a weak band correlating with an intense band can gain considerable intensity in the cross-peak. In our calculation of the 2D FT-IR spectrum shown in Fig. 16, the numerical threshold was set too high for the wagging sequence $\gamma_w(CH_2)$ (see Sec. 3.2.3). Therefore $\gamma_w(CH_2)$ did not result in autopeaks on the diagonal of the 2D FT-IR spectrum. Nevertheless there are two rows of seven cross-peaks correlating with the split $\nu_{as}(COO^-)$ band and the $\gamma_w(CH)_2$ sequence. This demonstrates that 2D correlation analysis is able to detect weak bands, provided they correlate with an intense band. The second example demonstrates a very critical aspect of 2D correlation analysis, namely, the principle impossibility of detecting the correct polarity, i.e., of reporting the correct correlation of a weak band overlapped by a strong band of opposite polarity. This is the case with the narrow CH_2 bending band $\delta(CH_2)$ at 1470 cm^{-1} which is assigned to the protonated form of arachidic acid; see Fig. 10A. The broad band with opposite sign around 1470 cm^{-1} determines numerically the sign of $\delta(CH_2)$ and consequently disables the correlation analysis to give the correct answer.

The problem of finding correlated populations is much simpler and considerably more reliably solved by consulting the basic data, namely, the phase-

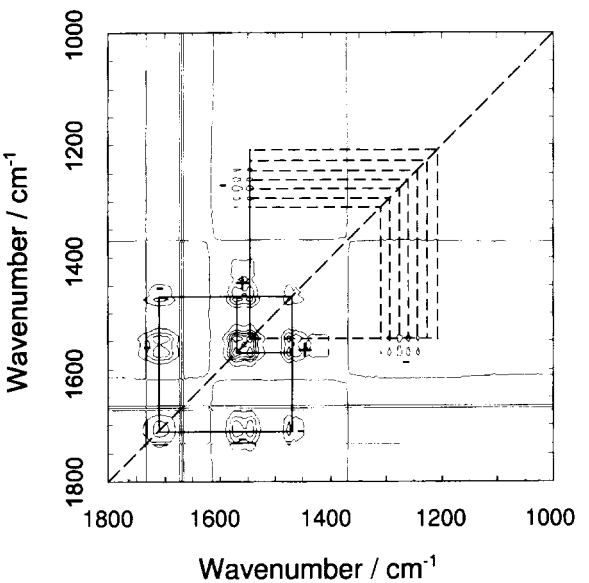

Fig. 16 Synchronous 2D FT-IR spectrum of an arachidic acid (ArAc) bilayer attached to a germanium internal reflection element (IRE) influenced by pH-modulated excitation (ME). The 0° and 90° modulation spectra of Fig. 10A were used for calculation of this 2D plot according to Ref. 18. On the dashed diagonal are the positive peaks of the autocorrelation function, which coincide with the wavenumbers of the absorbance spectrum (see Fig. 10). The plus and minus signs in the figure denote the sign of the cross-peak. A positive cross-peak means that the two signals on the diagonal are in phase (positive correlation); a negative cross-peak means out of phase (negative correlation), i.e., exhibiting in this experiment exactly 0° and 180° phase differences (see Sec. 3.2.3). Note the two rows of weak negative cross-peaks, although no autopeaks are visible between 1200 and 1300 cm^{-1}. The frequencies coincide with those of the wagging sequence. These cross-peaks gain their intensity from the most intense band in the spectrum, the split antisymmetric carboxylate stretching band $\nu_{as}(COO^-)$. A second phenomenon should be mentioned. Looking at the CH_2 bending vibration at 1470 cm^{-1}, there is a positive correlation (0°) with $\nu_{as}(COO^-)$ and a negative one (180°) with C=O stretching of the carboxyl group ν(COOH). This finding is not completely correct, since, as quickly verified from Fig. 10A, there is a weak narrow band at 1470 cm^{-1}, which is in phase with ν(COOH) and out of phase with $\nu_{as}(COO^-)$. This fact cannot be detected by 2D FT-IR plots, since numerically the polarity of the narrow band is falsified due to overcompensation by a more intense band of opposite sign. See also the text.

resolved modulation spectra shown in Fig. 10. In this context, the reader is referred to Ref. 18.

5 SPECTROSCOPIC SIGNAL PROCESSING

A modulated perturbation of the sample by an external parameter leads to periodic changes in the concentration $c_i(t)$ of the excited species A_i, resulting in modulated alterations of the absorbance of this species. However, changes of the sample thickness $d(t)$, e.g., by stretching or hydration, or changes of the absorption coefficient $\varepsilon_i(\tilde{\nu}, t)$ itself, e.g., due to temperature modulation, can also can also contribute to the time-dependent absorption.

Regarding the common case of a constant absorption coefficient $\varepsilon_i(\tilde{\nu})$ and a constant thickness d, Lambert–Beer's law leads to the measured time-dependent absorption of the species A_i,

$$A_i(\tilde{\nu}, t) = \varepsilon_i(\tilde{\nu}) \cdot c_i(t) \cdot d \tag{24}$$

Due to Fourier's theorem, the periodic function $c_i(t)$ can always be expressed by a Fourier series in the form

$$c_i(t) = c_{i,0} + \sum_{k=1}^{\infty} c_{i,k} \sin(k\omega t + \varphi_{i,k}) \tag{25}$$

where k denotes the multiple of the fundamental ($k = 1$ fundamental frequency, $k > 1$ higher harmonics) and $c_{i,0}(t)$ is the mean concentration in the stationary state. $c_{i,k}$ and $\varphi_{i,k}$ are the required data for kinetic analysis representing the amplitudes and phase lags of the kth harmonic, respectively. To simplify the following algorithm, we use a periodic excitation Eq. (1), with a phase $\theta = -\pi/2$, which leads to the harmonic stimulation

$$\eta(t) = \eta_0 + \Delta\eta_0 + \Delta\eta_1 \cos\left(\omega t - \frac{\pi}{2}\right) = \eta_1 + \Delta\eta_0 + \Delta\eta_1 \sin(\omega t) \tag{26}$$

This stimulation function results in measured phase shifts corresponding directly to the phase lags $\varphi_{i,k}$ introduced by the system itself (Eq. (25)).

Assuming N reacting species, Eq. 24 must be completed to describe the overall absorbance by

$$A(\tilde{\nu}, t) = \sum_{i=1}^{N} A_i(\tilde{\nu}, t) \tag{27}$$

The evaluation of $c_{i,k}$ and $\varphi_{i,k}$ from the measured time-dependent absorption $A(\tilde{\nu}, t)$ is the subject of phase-sensitive detection (PSD).

5.1 Principles of Phase-Sensitive Detection

Phase-sensitive detection is used to detect small periodic signals in a noisy background or to separate them from large and noisy background signals, as often encountered in spectroscopy. As stated earlier, the changes in the absorbance due to modulated excitation are periodic, exhibiting the period of the stimulation. Therefore, they can be expressed by a Fourier series:

$$A(\tilde{\nu}, t) = \sum_{i=1}^{N} A_{i,0}(\tilde{\nu}) + \sum_{i=1}^{N} \sum_{k=1}^{\infty} A_{i,k}(\tilde{\nu}) \sin(k\omega t + \varphi_{i,k}) \tag{28}$$

The first part of the right-hand side of Eq. (28) results in the stationary overall absorbance of the system, while the second part contains the modulated response. The amplitude $A_{i,k}(\tilde{\nu})$ is associated with the group of absorption bands exhibiting the same phase angle $\varphi_{i,k}$ at frequency $k\omega$.

Such a group may be assigned to species A_i and is referred to as the ith population. In the simplest case, we have to consider at least two populations, one of the reactants, the other of the products.

In order to determine the kth amplitude $A_{i,k}(\tilde{\nu})$ and the corresponding phase lag $\varphi_{i,k}$, the periodic function $A(\tilde{\nu}, t)$ is multiplied by a function $\sin(k\omega t + \phi_k^{PSD})$ and integrated over a period of the stimulation $T = 2\pi/\omega$. The factor of $2/T$ is necessary for normalization, i.e., to match the amplitudes before and after PSD. After some straightforward calculation, this leads to the phase-resolved absorbance spectrum $A_k(\tilde{\nu}, \phi_k^{PSD})$ with ϕ_k^{PSD} as parameter:

$$\begin{aligned} A_k(\tilde{\nu}, \phi_k^{PSD}) &= \sum_{i=1}^{N} A_{i,k}(\tilde{\nu}, \phi_k^{PSD}) = \frac{2}{T}\int_0^T A(\tilde{\nu}, t) \sin(k\omega t + \phi_k^{PSD}) dt \\ &= \sum_{i=1}^{N} A_{i,k}(\tilde{\nu}) \cos(\varphi_{i,k} - \phi_k^{PSD}) \end{aligned} \tag{29}$$

The parameter ϕ_k^{PSD} can be selected by the operator. Obviously the amplitude $A_{i,k}(\tilde{\nu}, \phi_k^{PSD})$ becomes maximum for $\phi_k^{PSD} = \varphi_{i,k}$ resulting in the unknown amplitude $A_{i,k}(\tilde{\nu})$. On the other hand, if $\phi_k^{PSD} = \varphi_{i,k} \pm 90°$, the cosine function and thus the amplitude $A_{i,k}$ become zero. Consequently, maximizing $A_{i,k}(\tilde{\nu}, \phi_k^{PSD})$ by variation of ϕ_k^{PSD} results in both the amplitude $A_{i,k}(\tilde{\nu})$ and the phase lag $\varphi_{i,k}$ of the response of the ith population to frequency $k\omega$.

5.2 Application of Phase-Sensitive Detection in Spectroscopy

As shown by Eq. (29), the time-dependent absorbance has to be multiplied by a trigonometric function and integrated over a period of stimulation to perform the

PSD. It should be noted that the primary signal measured in FT-IR spectroscopy is the interferogram representing the intensity of the IR beam as a function of the interferometer retardation. Therefore, the results of a PSD performed on the IR beam intensity during sampling of the interferogram does not give the same result as a PSD performed in the time-dependent absorbance domain. The reason is the logarithmic relation between intensity and absorbance according to Lambert–Beer's law:

$$I_i(\tilde{\nu}, t) = I_{0,i}(\tilde{\nu}, t) \cdot 10^{-A_i(\tilde{\nu},t)} \tag{30}$$

This nonlinear relation between intensity and absorbance (i.e., concentration) leads to systematic errors as soon as the exponential no longer admits a linear approximation. In this case, a logarithmic amplifier or application of sophisticated mathematical procedures is required. Nevertheless, PSD of many reported FT-IR experiments using modulation spectroscopy were performed in the interferogram domain. Most of these applications used the step-scan mode, with an additional phase modulation by means of the interferometer moving mirror. Consequently, two PSD steps were necessary for complete demodulation (35–38). Up to the time when digital signal processing (DSP) became fast enough, analog lock-in amplifiers were used to perform the PSD. In a first step, lock-in amplifiers were replaced by external digital signal processing (39) or digital lock-in amplifiers. In current developments, the digital signal processor circuits of the spectrometers are used to replace external digital signal processing (12,40).

In our laboratory, we use a digital PSD via software, performed after the sampling of time-resolved absorbance spectra is completed (41). The advantage of this method is the separation of data sampling (including FT-IR phase correction) and the PSD. The data sampling can therefore be done in every time-resolved measurement mode, which is essential for long-period modulation experiments. Application is also possible without step-scan equipment. However, the highest-modulation frequency, which determines time resolution, is then limited by the scan velocity, unless more sophisticated techniques, such as interleaved rapid scan, are applied. Moreover, all of the time-dependent information is still available after the experiment, enabling demodulation at any multiple of the stimulation frequency and at any PSD phase setting. The synchronized sampling and coaddition of time-resolved spectra $A(\tilde{\nu}, t)$ during the modulation period is a requirement of this method (41,42). Concerning data acquisition, $A(\tilde{\nu}, t)$ is an array of n absorbance spectra $\{A(\tilde{\nu}, t_1), A(\tilde{\nu}, t_2), \ldots, A(\tilde{\nu}, t_n)\}$ measured with a time interval $\Delta t = T/n$. Accordingly, the basic integral of PSD Eq. (29) becomes discrete:

$$A_k(\tilde{\nu}, \phi_k^{PSD}) = \frac{1}{C} \sum_{m=0}^{n-1} A(\tilde{\nu}, t_m) \sin[k\omega(m\Delta t) + \phi_k^{PSD}] \tag{31}$$

where C is a factor for normalization depending on the method of numerical integration. It should be mentioned that $A(\tilde{\nu}, t_m)$ denotes the mth entire spectrum. For that reason, the PSD is performed as a vector PSD and leads immediately to the phase-resolved spectra $A_k(\tilde{\nu}, \phi_k^{PSD})$.

The modulation amplitude and phase lag at a given wavenumber $\tilde{\nu}^*$ can now be determined by varying the phase of the PSD until the absorbance at $\tilde{\nu}^*$ in the phase-resolved spectrum becomes maximum. For non-overlapping bands, the amplitudes and phase lags of all bands can easily be calculated from two orthogonal phase-resolved spectra e.g., $A_k(\tilde{\nu}, 0°)$ and $A_k(\tilde{\nu}, 90°)$, which are also called in-phase and out-of-phase spectra, respectively. The modulation amplitude results from

$$A_k(\tilde{\nu}) = \sqrt{[A_k(\tilde{\nu}, 0°)]^2 + [A_k(\tilde{\nu}, 90°)]^2} \tag{32}$$

To calculate the absolute phase lag in the range of 0°–360°, one has to consider that the result of the arctan function is defined to be only within −90° and 90°, because $\tan \varphi = \tan(\varphi + 180°)$. Table 1 shows how to calculate the absolute phase lag φ_k in the range from 0° to 360°.

5.3 Phase Resolution of Overlapping Bands

In the case of overlapping bands, modulation spectroscopy can help to discriminate single components if the kinetics and, therefore, also the phase lags of overlapping bands are different. In this case the calculation of a set of phase-resolved spectra with different PSD-phase settings is very helpful (see Figs. 4B and 5B).

Let us consider two absorbing species with different phase lags α and β. According to Eq. (29), there is always a PSD phase setting resulting in zero absorbance for species A_i. For a species with phase lag α this is the case for $\phi_k^{PSD} = \alpha \pm 90°$. If, as assumed, the second species exhibits a different phase

Table 1 Calculation of the Phase Lag $\varphi_k(\tilde{\nu})$ (Absolute Phase Lag) Considering the Non-determined Range of the Arctan Function within 0° and 360°

$\varphi_{k,\text{absolute}}$	$A_k(\tilde{\nu}, 0°)$	$A_k(\tilde{\nu}, 90°)$
$\varphi_k = \arctan\left(\frac{A_k(\tilde{\nu}, 90°)}{A_k(\tilde{\nu}, 0°)}\right)$	≥ 0	≥ 0
$\varphi_k = \arctan\left(\frac{A_k(\tilde{\nu}, 90°)}{A_k(\tilde{\nu}, 0°)}\right) + 360°$	≥ 0	< 0
$\varphi_k = \arctan\left(\frac{A_k(\tilde{\nu}, 90°)}{A_k(\tilde{\nu}, 0°)}\right) + 180°$	< 0	$\forall\, A_k(\tilde{\nu}, 90°)$

lag β, its modulation spectrum $A_k(\tilde{\nu}, \alpha \pm 90°)$ will not vanish at this phase setting. In this simple case, the remaining absorbance results only from the species with phase lag β; i.e., separation has been achieved on a completely experimental level. By analogous procedure, the decoupled state of the species with phase lag α is achieved at PSD phase setting $\phi_k^{PSD} = \beta \pm 90°$, resulting in the phase-resolved spectrum $A_k(\tilde{\nu}, \beta \pm 90°)$, which is free of overlapping by absorption bands of the other species.

A typical example should be given: Considering the phase-resolved T-ME spectra shown in Figs. 5B and C, we realize that in the fundamental (ω) spectrum with phase setting $\phi_{PSD} = 135°$, the intense bands of the helix at 1639 cm^{-1} and of the antiparallel β-sheet at 1614 and 1685 cm^{-1} are virtually absent, indicating that these dominant signals exhibit phase lags of 135° ± 90°. However, the remaining modulation spectrum unambiguously shows two weak sigmoidal bands at 1614/1609 cm^{-1} and 1685/1680 cm^{-1}, pointing to an intermediate antiparallel β-structure, possibly a precursor of the final state at 1614 cm^{-1} and 1685 cm^{-1}, which is visible in the other modulation spectra and in the stationary spectrum, Fig. 5A. The existence of this intermediate species is confirmed by the first harmonic (2ω) modulation spectrum at the $\phi_{PSD} = 0°$ setting; see Fig. 5C. Moreover, its intense response in the first harmonic, while excitation has been performed in the fundamental frequency ω, gives strong evidence for second-order kinetics with large amplitudes, as expected for intermediates of a phase transition.

6 KINETICS OF PERIODICALLY EXCITED SYSTEMS

6.1 The Simplest Case of a Reversible First-Order Reaction

As an example of a kinetic analysis using modulation technique we will demonstrate the procedures for a reversible first-order reaction of the type

$$A_1 \underset{k_-}{\overset{k_+}{\rightleftharpoons}} A_2 \tag{33}$$

which may be typical for a simple conformational change, e.g. a cis-trans isomerization.

The rate equations $c_i(t)$ $(i = 1, 2)$ are given by

$$\dot{c}_1(t) = -k_+ c_1(t) + k_- c_2(t), \qquad \dot{c}_2(t) = k_+ c_1(t) - k_- c_2(t) \tag{34}$$

where $c_i(t)$ denotes time-dependent concentrations of the species $\mathbf{A}_i$ and k_+ and k_- are the rate constants of the forward and the backward reaction, respectively. Introducing the extent of reaction $\xi(t)$ as a relevant parameter that is related to concentrations according to

$$c_i(t) = c_{i,0} + \nu_i \xi(t) \tag{35}$$

where c_i and $c_{i,0}$ denote the actual and the initial concentration of the ith species, respectively, and ν_i is the stoichiometric number, which is, according to convention, negative for reactants and positive for products (44). Thus it follows for the concentrations of A_1 and A_2

$$c_1(t) = c_{1,0} - \xi(t), \qquad c_2(t) = c_{2,0} + \xi(t) \tag{36}$$

The rate equation in terms of the extent of reaction follows from combining Eqs. (34) and (36):

$$\dot{\xi}(t) = -(k_+ + k_-)\xi(t) + k_+ c_{1,0} - k_- c_{2,0} \tag{37}$$

Up to now, no external stimulation was considered. In order to describe a temperature-modulated excitation with small amplitudes, we introduce the temperature-dependent rate constants, as given by Eq. (4). Furthermore, to shorten the notations, abbreviations with distinct physical meaning, summarized by Eq. (38), are introduced:

$$\begin{aligned}
\varkappa_1 &= k_+ + k_- + \frac{\Delta T_0}{T_0^2}(T_{A_+}k_+ + T_{A_-}k_-) = \bar{k}_+ + \bar{k}_- \\
\varkappa_2 &= \frac{\Delta T_1}{T_0^2}(T_{A_+}k_+ + T_{A_-}k_-) = \Delta k_+ + \Delta k_- \\
\varkappa_3 &= c_{2,0}k_- - c_{1,0}k_+ + \frac{\Delta T_0}{T_0^2}(T_{A_-}c_{2,0}k_- - T_{A_+}c_{1,0}k_+) = c_{2,0}\bar{k}_- - c_{1,0}\bar{k}_+ \\
\varkappa_4 &= \frac{\Delta T_1}{T_0^2}(T_{A_-}c_{2,0}k_- - T_{A_+}c_{1,0}k_+) = c_{2,0}\Delta k_- - c_{1,0}\Delta k_+
\end{aligned} \tag{38}$$

$\bar{k}_+ + \bar{k}_-$ denotes the sum of the rate constants at the stationary (mean) temperature $T_0 + \Delta T_0$, while rate constants without overbars relate throughout to the initial temperature T_0. Δk_+ and Δk_- denote the change of the corresponding rate constants resulting from a temperature change equal to the modulation amplitude ΔT_1; see also Fig. 1.

The differential equation of the periodically excited system results:

$$\dot{\xi}(t) + [\varkappa_1 + \varkappa_2 \cos(\omega t + \theta)] \cdot \xi(t) + \varkappa_3 + \varkappa_4 \cos(\omega t + \theta) = 0 \tag{39}$$

This equation has no exact analytical solution, because of the time-dependent part $\varkappa_2 \cos(\omega t + \theta)$ in the coefficient of $\xi(t)$. Because we assumed small modulation amplitudes ΔT_1, this part can be neglected, which is confirmed by a numerical solution of Eq. (39). The approximate rate equation thus results in

$$\dot{\xi}(t) + \varkappa_1 \cdot \xi(t) + \varkappa_3 + \varkappa_4 \cos(\omega t + \theta) = 0 \tag{40}$$

The solution of this differential equation is

$$\xi(t) = -\frac{\varkappa_3}{\varkappa_1} + \left[\frac{\varkappa_3}{\varkappa_1} + \frac{\varkappa_1\varkappa_4 \cos\theta + \varkappa_4\omega \sin\theta}{\varkappa_1^2 + \omega^2}\right] \cdot e^{-\varkappa_1 t} \tag{41}$$

$$- \frac{\varkappa_4}{\varkappa_1^2 + \omega^2} [\varkappa_1 \cos(\omega t + \theta) + \omega \sin(\omega t + \theta)]$$

$\xi(t)$ consists of a constant term, an exponentially relaxing term, and a modulated term. The time-dependent trigonometric expression in brackets may be reduced to a cosine function with phase shift, in analogy to Fourier series (43). It follows that

$$\varkappa_1 \cos(\omega t + \theta) + \omega \sin(\omega t + \theta) = \sqrt{\varkappa_1^2 + \omega^2} \cos(\omega t + \theta + \varphi)$$

where

$$\cos\varphi = \frac{\varkappa_1}{\sqrt{\varkappa_1^2 + \omega^2}} \quad \text{and} \quad \sin\varphi = -\frac{\omega}{\sqrt{\varkappa_1^2 + \omega^2}} \tag{42}$$

$$\text{or} \quad \tan\varphi = -\frac{\omega}{\varkappa_1}$$

Denoting the corresponding magnitudes by ξ_c, $\xi_r(\omega, \theta)$, and $\xi_m(\omega, \theta)$, respectively, and taking account of Eq. (42), Eq. (41) may be rewritten in the form

$$\xi(t) = \xi_c + \xi_r(\omega, \theta)\, e^{-(\bar{k}_+ + \bar{k}_-)t} + \xi_m(\omega, \theta) \cos(\omega t + \theta + \varphi) \tag{43}$$

φ denotes the phase lag introduced by the delayed system response, and $\xi_m(\omega, \theta)$ denotes the amplitude of the modulated part of the extent of reaction. In the notation given by Eq. (43), $\xi_m(\omega, \theta)$ may be positive or negative depending on the sign of $\varkappa_4$ (see Eq. (38)). Consequently, the phase angle introduced by the system may assume the value φ or $\varphi \pm \pi$. A method to determine the absolute value of φ is indicated later.

Direct relations to relevant quantities in kinetics are now obtained by combining Eqs. (38), (41), and (43). In the stationary state of modulated excitation, the time mean of the extent of reaction $\xi(t)$ results in the constant term ξ_c:

$$\xi_c = \frac{c_{1,0}\bar{k}_+ - c_{2,0}\bar{k}_-}{\bar{k}_+ + \bar{k}_-} \tag{44}$$

ξ_c describes the extent of reaction between the initial equilibrium state at $T = T_0$ and the stationary state, which corresponds to a new equilibrium state at $T = T_0 + \Delta T_0$. Note that ξ_c becomes zero if the initial concentrations $c_{1,0}$ and $c_{2,0}$ are already equilibrium concentrations at $T = T_0 + \Delta T_0$, as expected and as may be verified by considering the rate Eq. (34) at zero rate, which means equilibrium.

$\xi_r(\omega, \theta)$, from the second term of Eq. (43), denotes the magnitude of the exponentially declining part of the extent of reaction. This part of the general solution is not used in modulation spectroscopy; however, it is of interest for

comparison with corresponding results from T-jump experiments (3). In a first view, Eq. (43) indicates that the relaxation time results in

$$\tau_m = \frac{1}{\bar{k}_+ + \bar{k}_-} = \frac{1}{(k_+ + \Delta k_+) + (k_- + \Delta k_-)} \tag{45}$$

where k_+ and k_- are the rate constants at $T = T_0$ and Δk_+ and Δk_- denote the changes of rate constants induced by the temperature change between initial state T_0 and stationary state $T_0 + \Delta T_0$. In relaxation spectroscopy, the relaxation time τ_r is usually related to the initial temperature T_0; i.e., $\tau_r = 1/(k_+ + k_-)$. The difference between τ_m and τ_r, however, is small and may be calculated via Eq. (38).

Taking the reduction introduced by Eq. (42) into account, one obtains for the magnitude of ξ_r

$$\xi_r = \frac{c_{2,0}\bar{k}_- - c_{1,0}\bar{k}_+}{\bar{k}_+ + \bar{k}_-} + \frac{(c_{2,0}\Delta k_- - c_{1,0}\Delta k_+)\cos(\theta + \varphi)}{\sqrt{(\bar{k}_+ + \bar{k}_-)^2 + \omega^2}} \tag{46}$$

The first term on the right-hand side of this equation is a constant that is equal to $-\xi_c$. If we combine it with Eq. (44) we get the portion of $\xi(t)$ corresponding to the T-jump relaxation; i.e.,

$$\xi_{\text{jump}} = \xi_c[1 - e^{-(\bar{k}_- + \bar{k}_-)t}] = \xi_c[1 - e^{-t/\tau_m}] \tag{47}$$

This equation demonstrates that relaxation and modulation techniques contain the same kinetic information on relaxation times and amplitudes.

The second term of Eq. (46) depends on modulation amplitude and frequency ω as well as on the phase angle θ of the stimulation (see Eq. (1)) and on the phase lag φ introduced by the delayed response of the system. This part describes the phase relaxation of the response. Because concentration relaxation (ξ_{jump}) vanishes when initial concentrations are equal to stationary concentrations, phase relaxation vanishes when the phase angle θ of the stimulation differs by $\pm 90°$ from the system phase lag φ. In practice, however, this condition cannot be fulfilled. Consequently, data acquisition for modulation spectroscopy should be started no earlier than $3\tau_m$ after the beginning of stimulation; otherwise, a systematic error due to a contribution of nonstationary response will occur.

Phase relaxation also vanishes at high modulation frequencies, which means $\omega \gg (\bar{k}_+ + \bar{k}_-)$; however, as will be shown later, the amplitudes of the modulated responses also will vanish under this condition.

Considering now the third term in Eq. (43), we may express the amplitude in the form

$$|\xi_m(\omega)| = \frac{|c_{1,0}\Delta k_+ - c_{2,0}\Delta k_-|}{|\sqrt{(\bar{k}_+ + \bar{k}_-)^2 + \omega^2}|} = \frac{|c_{1,0}\Delta k_+ - c_{2,0}\Delta k_-| \cdot \tau_m}{|\sqrt{1 + (\omega\tau_m)^2}|} \tag{48}$$

As already mentioned (Eq. (45)), $\tau_m = (\bar{k}_+ + \bar{k}_-)^{-1}$ denotes the relaxation time of reaction shown by Eq. (33). Equation (48) results in the absolute value of the

modulation amplitude. It should be noted, however, that the amplitude may be positive or negative, depending on the magnitudes of the products between initial concentrations $c_{1,0}$ and $c_{2,0}$ and the change of rate constants under the influence of the modulation amplitude ΔT_1, namely, Δk_+ and Δk_-, which depend on the activation energies of forward and backward reactions, respectively. We take the sign of the amplitude via the phase lag φ into account, resulting in Eq. (49), which is a modification of the trigonometric functions of the phase lag indicated in Eq. (42):

$$\begin{aligned}
\cos\varphi &= \frac{\operatorname{sign}(c_{1,0}\Delta k_+ - c_{2,0}\Delta k_-)\cdot(\bar{k}_+ + \bar{k}_-)}{|\sqrt{(\bar{k}_+ + \bar{k}_-)^2 + \omega^2}|} \\
&= \frac{\operatorname{sign}(c_{1,0}\Delta k_+ - c_{2,0}\Delta k_-)}{|\sqrt{1 + (\omega\tau_m)^2}|} \\
\sin\varphi &= -\frac{\operatorname{sign}(c_{1,0}\Delta k_+ - c_{2,0}\Delta k_-)\cdot\omega}{|\sqrt{(\bar{k}_+ + \bar{k}_-)^2 + \omega^2}|} \\
&= -\frac{\operatorname{sign}(c_{1,0}\Delta k_+ - c_{2,0}\Delta k_-)\cdot\omega\tau_m}{|\sqrt{1 + (\omega\tau_m)^2}|} \\
\tan\varphi &= -\frac{\omega}{\bar{k}_+ + \bar{k}_-} = -\omega\tau_m
\end{aligned} \tag{49}$$

It should be noted that the right quadrant for the phase angle φ can be determined only by considering the signs of two trigonometric functions indicated in Eq. (49), as depicted in Table 2.

Finally, the modulated part of the stationary solution (subscript m, stat) of $\xi(t)$ may be written in the form

$$\xi_{m,\mathrm{stat}}(t) = \frac{|c_{1,0}\Delta k_+ - c_{2,0}\Delta k_-|\cdot\tau_m}{|\sqrt{1 + (\omega\tau_m)^2}|}\cos(\omega t + \theta + \varphi) \tag{50}$$

where the phase angle has to be determined from Eq. (49) and Table 2.

As an illustration, the time-dependent concentration $c_2(t)$ of species A_2 (see Eq. (36)) was calculated and is shown in Fig. 17A. The frequency dependence

Table 2 Signs of the Trigonometric Functions

Quadrant	sin	cos	tan
I	+	+	+
II	+	−	−
III	−	−	+
IV	−	+	−

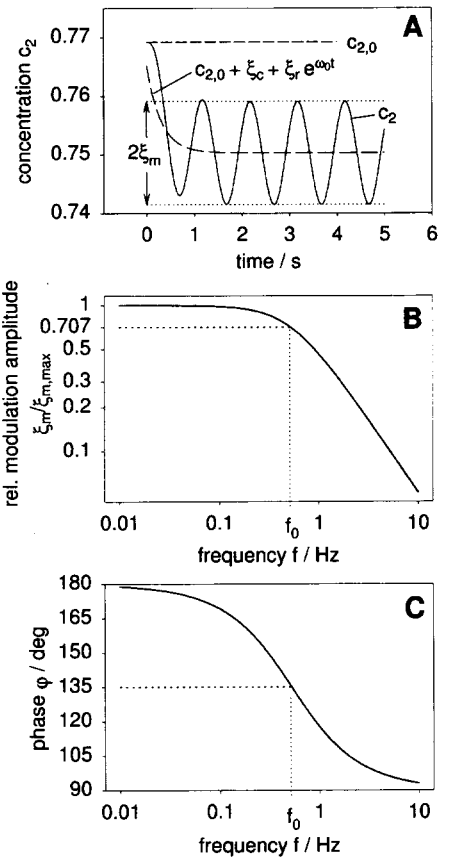

Fig. 17 Kinetics of a temperature-modulated model system. The concentration c_2 of the product in reaction $A_1 \rightleftarrows A_2$ is calculated as a function of time using Eqs. (36) and (50) (A). The mean value of the concentration decreases exponentially, caused by the temperature jump ΔT_0. After a few periods, the stationary state is reached, exhibiting the changes in concentration due to the temperature modulation amplitude ΔT_1. With increasing frequency the modulation amplitude ξ_m decreases, assuming a slope of -6 dB per octave at elevated frequency according to Eq. (48) (B), and the phase lag φ (C) decreases according to Eq. (49). At the frequency f_0, the amplitude ξ_m has decreased by a factor of $1/\sqrt{2}$ (-3 dB). The phase lag at the 3-dB point results in $\varphi = 3\pi/4$ (C). The parameters used for calculation were: $E_{a,+} = 35{,}000$ J/mol, $E_{a,-} = 55{,}000$ J/mol, $k_+ = 2\ s^{-1}$, $k_- = 0.6\ s^{-1}$, $T_0 = 298$ K, $\Delta T_0 = 5$ K, $\Delta T_1 = 5$ K, $f = 1$ Hz, and $\theta = -\pi$.

of the modulation amplitude $|\xi_m(\omega, \theta)|$ and the phase lag $\varphi(\omega)$ as calculated by Eqs. (48) and (49) are shown in Figs. 17B and C.

6.2 Evaluation of Kinetic Parameters from Spectroscopic Modulation Experiments

In Sec. 6.1 the solution in terms of the extent of reaction ξ was derived for a T-ME of the simple reaction scheme depicted by Eq. (33). It is related to the concentration of the reacting species according to Eqs. (35) and (36). Data acquisition, on the other hand, leads to absorbances $A_i(\tilde{\nu}, t)$, which are related to concentrations by Lambert–Beer's law, Eq. (24). Taking into account that data acquisition in modulation spectroscopy is performed in the stationary state of excitation, the relaxation term in Eq. (43) can be omitted, resulting in

$$\begin{aligned} A_{i,\mathrm{stat}}(\tilde{\nu}, t) &= \varepsilon(\tilde{\nu}) \cdot d \cdot c_i(t) = \varepsilon(\tilde{\nu}) \\ &\quad \cdot d \cdot (c_{i,0} + \nu_i \cdot (\xi_c + |\xi_m(\omega, \theta)| \cos(\omega t + \theta + \varphi_i) \end{aligned} \tag{51}$$

Note that φ_i now denotes the phase of species A_i. In this example, φ_i and the phase of the extent of reaction φ are equal if the corresponding species is the product A_2. However, they are out of phase if the ith species is a reactant, e.g., A_1. Consequently, Eq. (49), which indicates the absolute phase of the extent of reaction, has to be modified as follows in order to get the phase of a distinct species A_i:

$$\begin{aligned} \cos \varphi_i &= \frac{\mathrm{sign}(\nu_i) \cdot \mathrm{sign}(c_{1,0}\Delta k_+ - c_{2,0}\Delta k_-)}{|\sqrt{1 + (\omega\tau_m)^2}|} \\ \sin \varphi_i &= -\frac{\mathrm{sign}(\nu_i) \cdot \mathrm{sign}(c_{1,0}\Delta k_+ - c_{2,0}\Delta k_-) \cdot \omega\tau_m}{|\sqrt{1 + \omega\tau_m)^2}|} \\ \tan \varphi_i &= -\mathrm{sign}(\nu_i) \cdot \frac{\omega}{\bar{k}_+ + \bar{k}_-} = -\mathrm{sign}(\nu_i) \cdot \omega\tau_m \end{aligned} \tag{52}$$

As a consequence of Eq. (52), the absolute value of the stoichiometric number ν_i has to be used from now on.

After PSD is performed for the fundamental frequency ($k = 1$) on $A_{i,\mathrm{stat}}(\tilde{\nu}, t)$, one obtains, from Eqs. (29) and (51),

$$A_{i,1} = \varepsilon(\tilde{\nu}) \cdot d \cdot |\nu_i| \cdot |\xi_m(\omega, \theta)| \sin(\phi_1^{PSD} - \theta - \varphi_i) \tag{53}$$

Introducing $\theta = -\pi/2$, as in Sec. 5, Eq. (26), which means stimulation with a sine function without phase shift, and solving Eq. (53) for the phase-resolved extent of reaction leads to

$$|\xi_{m,1}(\omega, \theta)| \cos(\varphi_i - \phi_1^{PSD}) = \frac{A_{i,1}(\tilde{\nu}, \phi_1^{PSD})}{|\nu_i| \cdot \varepsilon(\tilde{\nu}) \cdot d} \tag{54}$$

It should be noted that digital PSD results in the phase-resolved modulation spectra $A_{i,1}(\tilde{\nu}, \phi_1^{PSD})$ at any PSD phase setting ϕ_1^{PSD}. In case of the reversible first-order

reaction (Eq. (33)), one can conclude directly from Eq. (52) that the reactant A_1 and the product A_2 exhibit a relative phase difference of 180°, since $\nu_1 = -1$, and $\nu_2 = +1$.

In order to determine the relevant quantities $|\xi_{m,1}(\omega, \theta)|$ and φ_i, the minimum expenditure is to perform modulation experiments at a frequency in the range $0.1 < \omega \cdot \tau_m < 10$. $|\xi_{m,1}(\omega, \theta)|$ and φ_i are then obtained, e.g., by the following procedure:

1. Look for the distinct PSD phase setting $\phi^{PSD}_{1,\text{zero}}$, which results in zero amplitude. At this setting it follows that $\varphi_i - \phi^{PSD}_{1,\text{zero}} = \pm 90°$, i.e., $\varphi_i = \phi^{PSD}_{1,\text{zero}} \pm 90°$. The absolute value of φ_i may be determined by means of Table 1 in Sec. 5.
2. Add $\pm 90°$ to $\phi^{PSD}_{1,\text{zero}}$. At this setting, $\phi^{PSD}_{1,\text{extreme}} = \phi^{PSD}_{1,\text{zero}} \pm 90°$, the cosine function on the left-hand side of Eq. (54), assumes $+1$ or -1, i.e., an extreme, leading directly to the amplitude $|\xi_{m,1}(\omega, \theta)| \cdot |\nu_i|$.

It should be mentioned, however, that variation of ω in the range $0.1 < \omega \cdot \tau < 10$ enables multiple access to $|\xi_{m,1}(\omega, \theta)|$ and φ_i, which leads to enhanced accuracy and more reliable validation of an assumed reaction scheme. So-called Bode diagrams are presented in Fig. 14 and Figs. 17B and C. The latter depict the amplitude and phase dependence on frequency for a reaction scheme shown by Eq. (33). If the Bode diagrams differ from Figs. 17B and C, as is the case in Fig. 14, it follows that the underlying chemical reaction scheme must be more complicated. For details, the reader is referred to Sec. 3.4 and to Refs. 1 and 9.

In a more complex situation with overlapping modulation bands, it is advisable to proceed with analysis in two steps. First, a lineshape analysis of distinct bands over a complete set of phase-resolved modulation spectra $A_{i,1}(\tilde{\nu}, \phi_1^{PSD})$ (e.g., at $\phi_1^{PSD} = 0°, 22.5°, 45°, \ldots, 180°$) is performed. In a second step, each distinct modulation band of this phase-resolved set has to be fitted with respect to $|\xi_{m,1}(\omega, \theta)|$ and φ_i according to Eq. (54). For a typical example the reader is referred to Ref. 18.

6.3 Evaluation of Rate Constants from Phase Lag and Modulation Amplitude

As discussed in Sec. 6.2, ME experiments give access to the relaxation times of a system via phase lag measurements and via the amplitude/frequency dependence. Reaction Eq. (33) exhibits one relaxation time τ_m. The number of relaxation times of a more complicated reaction system equals the number of eigenvalues λ_i of the kinetic matrix and is related to them by Eq. (55) (3):

$$\tau_i = -\frac{1}{\lambda_i} \tag{55}$$

λ_i is a function of the rate constants and in the case of non-first-order steps also of the initial concentrations of the corresponding reacting species. A number of relaxation times of distinct reactions have been calculated and summarized in Ref. 3 and 45.

In the case of reaction Eq. (33), the relaxation time is given by Eq. (45). In order to evaluate the single constants $\bar{k}_+$ and $\bar{k}_-$, a second, independent relation is necessary, e.g., ξ_c, the extent of reaction between the initial equilibrium state at $T = T_0$ and the stationary state at $T = T_0 + \Delta T_0$ as described by Eq. (44). It follows from Eqs. (44) and (45) that

$$\bar{k}_- = \frac{c_{1,0} - \xi_c}{(c_{1,0} + c_{2,0})\tau_m} \quad \text{and} \quad \bar{k}_+ = \frac{1}{\tau_m} - \bar{k}_- \tag{56}$$

Finally, some features concerning the Bode diagrams shown in Figs. 17B and C should be mentioned. Plotting the relative extent of reaction $|\xi_m(\omega)|/|\xi_m(0)|$ as calculated from Eq. (48) versus frequency, it follows that the frequency fulfilling the condition $\omega\tau_m = 1$ has a special meaning, we call it ω_0 or $f_0 = 2\pi\omega_0$. According to Eq. (48), at this frequency the amplitude has decreased by a factor of $1/\sqrt{2}$, which corresponds to -3 decibels (dB). At elevated frequency, the amplitude declines with a slope of 6 dB per octave, i.e., by a factor of 2 upon frequency doubling. Moreover, the phase lag of species 2 (Eq. (33)) as calculated by Eq. (52) is shown in Fig. 17C. In order to understand the traces and the scaling of coordinate axes of Fig. 17, we have to look at the input data used for calculation of this example. The initial equilibrium concentrations at $T = T_0 = 298$ K were $c_{1,0} = 0.231$ mol/L and $c_{2,0} = 0.769$ mol/L. Temperature displacement and modulation amplitudes were equal, $\Delta T_0 = \Delta T_1 = 5$ *K*, and the phase shift of temperature stimulation according to Eq. (1) was $\theta = -\pi$. The following activation energies have been used for calculation: $E_{a+} = 35$ kJ/mol and $E_{a-} = 55$ kJ/mol. A relevant quantity for amplitude and phase determination is $(c_{1,0}\Delta k_+ - c_{2,0}\Delta k_-) = -0.0624$, i.e. sign $(c_{1,0}\Delta k_+ - c_{2,0}\Delta k_-) = -1$ as calculated by Eq. (38), using the data indicated earlier. Now considering the product $\mathbf{A}_2$ of reaction Eq. (33) it follows that sign$(\nu_2) = +1$. Insertion of these data into the phase equations (52) results in the signs of the trigonometric functions; i.e. sign$(\cos \varphi_2) = -1$, sign$(\sin \varphi_2) = +1$, and sign$(\tan \varphi_2) = -1$. Taking two of these signs and consulting Table 2 results in the second quadrant to be relevant for φ_2. As follows now from Eq. (52), the phase of species 2 alters from 180° at $\omega = 0$ to 90° at $\omega = \infty$, which is shown by Fig. 17C. The absolute phase lag at the 3-dB point, where $\omega\tau_m = 1$, results in $\varphi_2 = 3/4\pi = 135°$. The phase behavior of the reactant $\mathbf{A}_1$ differs from the product $\mathbf{A}_2$ only insofar that sign$(\nu_1) = -1$. Consideration of Eq. (52) and Table 2 assigns the forth quadrant to the phase φ_1, i.e., from $3/2\pi$ to 2π. It should be noted that multiples of 2π may be added to φ without changing the absolute character.

Introducing $\varphi_1 = 7/4\pi$ and $\varphi_2 = 3/4\pi$ into Eq. (51) and setting $t = 0$

demonstrates that the response of the system is ahead of the stimulation. Although mathematically correct because of the 2π periodicity of the process, it is usual in practice to subtract 2π from the phases determined by the procedure just described. Consequently, we indicate the absolute phase lags of the species of reaction Eq. (33) as $\varphi_1 = -\pi/4$ and $\varphi_2 = -5/4\pi$.

7 CONCLUSIONS

Modulation spectroscopy, or modulated excitation (ME) spectroscopy, has been presented as an experimental tool for the very sensitive detection of periodic concentration changes in a system that has been stimulated by a periodic modulation of an external parameter. The high signal-to-noise ratio typically achieved with ME techniques is based on the narrowband characteristic of phase-sensitive detection (PSD). If a large and noisy signal contains weak amounts of a periodic component with distinct frequency, e.g., the frequency of excitation, PSD selectively demodulates this modulated part and converts it into a direct current (DC) output. On the other hand, the dominant rest of the signal will be canceled, because PSD converts it to an output with mean value zero.

Since demodulation occurs within each period, there is minimal influence of apparative and environmental instabilities.

There is a close analogy between ME spectroscopy and relaxation spectroscopy. The latter is initiated by a jumplike change of an external parameter. This leads to a relaxation of the equilibrium concentrations before jump to the new equilibrium concentrations after jump. In ME spectroscopy, on the other hand, relaxation from the initial equilibrium state to a stationary state is observed. This state is characterized by a periodic concentration modulation about the stationary mean values. Furthermore, if the modulation frequency is matched to system kinetics, which is the case if the modulation frequency is close to the reciprocal relaxation time, significant phase shifts between stimulation and system response will be observed. This phenomenon is paralleled by increased amplitude damping with increasing frequency. For a given reaction scheme, both phase shift and amplitude damping depend systematically on the relaxation times of the system.

Obviously, both methods, relaxation and modulated excitation, lead to system relaxation times, which can be related to basic kinetic constants. Two significant differences should be noted, however, because we think that they mean an advantage of the ME technique. The first one is frequency doubling by nonlinear systems. If a sinusoidal ME is exerted under adequate conditions to a chemical system, producing a response in the first harmonic, one can unambiguously conclude that non-first-order kinetics are involved in the stimulated process. A nonlinear system response may result from 2nd order kinetics or more complex reactions like cooperative phenomena encountered with phase transitions or protein folding. Of course, a non-linear system response is also expressed by the shape of a relaxation curve. The difference to ME techniques is, however, that PSD

enables a selective detection of higher harmonics without application of any fitting model. Validation of a given model is then performed by variation of the stimulation frequency, since both phase shifts and amplitudes of the concentrations of reacting species depend critically on the underlying reaction scheme. In practice, procedures developed for electronic circuit analysis, such as Bode and Nyquist diagrams (46), may be applied.

Finally, it should be noted that the advantage of narrow-band measurements just mentioned must be paid for by extended data acquisition time.

REFERENCES

1. HsH Günthard. Ber Bunsenges Phys Chem 78:1110–1115, 1974.
2. M Eigen, L De Maeyer. In: SL Friess, ES Lewis, A Weissberger, eds. Techniques of Organic Chemistry. Vol. 8. Part 2. New York: Wiley-Interscience, 1963, pp. 895–1054.
3. H Strehlow, W Knoche. Fundamentals of Chemical Relaxation. Weinheim, Germany: Verlag Chemie, 1977.
4. I Noda. Appl Spectrosc 44:550–561, 1990.
5. UP Fringeli. In: Encyclopedia of Spectroscopy and Spectrometry. New York: Academic Press, 1999, pp. 58–75.
6. TL Hill. Thermodynamics for Chemists and Biologists. Reading, MA: Addison-Wesley, 1968.
7. J Monod, J Wyman, JP Changeux. J Mol Biol 12:88–118, 1965.
8. AA Frost, RG Pearson. Kinetics and Mechanism. 2nd ed. New York: Wiley, 1961, pp. 77–102.
9. M Forster, K Loth, M Andrist, UP Fringeli, HsH Günthard. Chem Phys 17:59–80, 1976.
10. O Kratky. Kolloid Z 64:213–222, 1933.
11. C Marcott, AE Dowrey, I Noda. Anal Chem 66:1065A–1075A, 1994.
12. C Marcott, GM Story, I Noda, A Bibby, CJ Manning. Pressure-modulation dynamic attenuated-total-reflectance (ATR) FT-IR spectroscopy. In: JA deHaseth, ed. Proceedings of the 11th International Conference on Fourier Transform Spectroscopy. Woodbury, NY: AIP Conference Proceedings 430, 1998, pp. 379–380.
13. D Blaudez, JM Turlet, D Dufourcq, D Bard, T Buffeteaux, B Desbat. J Chem Soc Faraday Trans 92:525–530, 1996.
14. D Blaudez, T Buffeteaux, JC Cornut, B Desbat, N Escafre, M Pezolet, JM Turlet. Thin Solid Films 242:146–150, 1994.
15. A Elliot, EJ Ambrose. Nature 165:921–922, 1950.
16. H Lenormant, ER Blout. Nature 172:770–771, 1953.
17. F Dousseau, M Pézolet. Biochemistry 29:8771–8779, 1990.
18. M Müller, R Buchet, UP Fringeli. J Phys Chem 100:10810–10825, 1996.
19. M Maroncelli, SP Qi, HL Strauss, RG Snyder. J Am Chem Soc 104:6237–6247, 1982.
20. H Casal, RN McElhaney. Biochemistry 29:5423–5427, 1990.
21. UP Fringeli, J Goette, G Reiter, M Siam, D Baurecht. Structural investigations of oriented membrane assemblies by FTIR-ATR spectroscopy. In JA deHaseth, ed. Proceedings of the 11th International Conference on Fourier Transform Spectroscopy. Woodbury, NY: AIP Conference Proceedings 430, 1998, pp. 729–747.

22. OPTISPEC, Rigistrasse 5, CH-8173 Neerach, Switzerland.
23. UP Fringeli. In: FM Mirabella Jr, ed. Internal Reflection Spectroscopy, Theory and Application. New York: Marcel Dekker, 1992, pp. 255–324.
24. P Hofer, UP Fringeli, WH Hopff. Biochemistry 23:2730–2734, 1984.
25. UP Fringeli, P Ahlström, C Vincenz, M Fringeli. Structure-activity relationships in enzymes: an application of IR-ATR modulation spectroscopy. Fourier and Computerized Infrared Spectroscopy, Montreal. Bellingham, WA: SPIE 553, 1985, pp. 234–235.
26. P Hofer, UP Fringeli. Biophys Struct Mech 6:67–80, 1979.
27. NB Colthup, LH Daly, SE Wiberley. Introduction to Infrared and Raman Spectroscopy. 3rd ed. New York: Academic Press, 1990.
28. F Kopp, UP Fringeli, K Mühlethaler, HsH Günthard. Z Naturforsch 30c:711–717, 1975.
29. W Münch, UP Fringeli, HsH Günthard. Spectrochim Acta 33A:95–109, 1977.
30. R Zbinden. Infrared Spectroscopy of High Polymers. New York: Academic Press, 1964.
31. G Cevc, D Marsh. Phospholipid Bilayers: Physical Principles and Models. New York: Wiley Interscience, 1987.
32. H Gerischer. In: P Delahay, ed. Advances in Electrochemistry and Electrochemical Engineering. New York: Wiley-Interscience, 1961, pp. 142–232.
33. P Delahay. Double Layer and Electrode Kinetics. New York: Wiley, 1965.
34. M Schwarzott, D Baurecht, UP Fringeli. Structural changes of PLL by electric field stimulation: an FTIR ATR modulation spectroscopic study. Structural Heterogeneity and Dynamics of Biological Macromolecules, Joint Meeting of the Dutch and German Biophysical Societies and the Biochemistry and Molecular Biology Society, May 13–16, 1999, Hünfeld, Germany, 1999, p. 88.
35. I Noda, AE Dowrey, C Marcott. Appl Spectrosc 42:203–216, 1988.
36. RA Crocombe, SV Compton. The Design, Performance and Application of a Dynamically Aligned Step-Scan Interferometer. FTS/IR Notes 82, Bio-Rad, Digilab Divison, Cambridge, MA, 1991.
37. RA Palmer. Spectroscopy 8:26–36, 1993.
38. RA Palmer, JL Chao, RM Dittmar, VG Gregoriou, SE Plunkett. Appl Spectrosc 47: 1297–1310, 1993.
39. CJ Manning, PR Griffiths. Appl Spectrosc 47:1345–1349, 1993.
40. R Curbelo. Digital signal processing (DSP) applications in FT-IR. Implementation examples for rapid- and step-scan systems. In JA deHaseth, ed. Proceedings of the 11th International Conference on Fourier Transform Spectroscopy. Woodbury, NY: AIP Conference Proceedings 430, 1998, pp. 74–83.
41. UP Fringeli. Int Pat Publ, PCT, WO 97/08598, 1997.
42. D Baurecht, W Neuhäuser, UP Fringeli. Modification of time-resolved step-scan and rapid-scan FTIR spectroscopy for modulation-spectroscopy in the frequency range from Hz to kHz. In: JA deHaseth, ed. Proceedings of the 11th International Conference on Fourier Transform Spectroscopy. Woodbury, NY: AIP Conference Proceedings 430, 1998, pp. 367–370.
43. CRC Standard Mathematical Tables. 18th ed. Cleveland, OH: Chemical Rubber Co, 1970.
44. I Mills, T Cvitas, K Homann, N Kallay, K Kuchitsu. Quantities, Units and Symbols in Physical Chemistry. Oxford: Blackwell Scientific, 1988, p. 38.
45. DN Hague. Fast Reactions. New York: Wiley-Intersciences, 1971.
46. HW Bode. Network Analysis. London: Van Nostrand Company, 1955.